Aus der

Neurologischen Universitätsklinik Tübingen

Abteilung Neurologie mit Schwerpunkt neurovaskuläre Erkrankungen

Real-Time Cognitive Output Modulation through EEG-triggered TMS

Inaugural-Dissertation
zur Erlangung des Doktorgrades
der Medizin

der Medizinischen Fakultät
der Eberhard Karls Universität
zu Tübingen

vorgelegt von
Song, Elina Fanglin

2025

Dekan:	Professor Dr. B. Pichler
1. Berichterstatter:	Professor Dr. U. Ziemann
2. Berichterstatter:	Professor Dr. M. Giese

Tag der Disputation: 02.06.2025

Meinen Eltern

A. Table of contents

B. Index of figures

C. List of abbreviations

APB	Abductor pollicis brevis
DMPFC	Dorsomedial prefrontal cortex
ECoG	Electrocorticography
EEG	Electroencephalography
EMG	Electromyography
EPSP	Excitatory postsynaptic potential
FDI	First dorsal interosseous
FM	Frontal-midline
fMRI	Functional magnetic resonance imaging
FPN	Frontoparietal network
IPSP	Inhibitory postsynaptic potential
IRASA	Irregular resampling auto-spectral analysis
LFP	Local field potential
LTM	Long-term memory
MEP	Motor evoked potential
MRI	Magnetic resonance imaging
PET	Positron emission tomography
PPC	Posterior parietal cortex
PSD	Power spectral density
RMT	Resting motor threshold
SNR	Signal-to-noise ratio
STM	Short-term memory
TMS	Transcranial magnetic stimulation
WM	Working memory

1 Introduction

1.1 Electroencephalography and neuronal oscillations

Effective neuronal activity occurs with oscillations, as groups of neurons are found to transfer information by synchronized activation. The synchronous activation of several neurons generates an electric field, which can be detected by electrodes placed in brain tissue (LFP), on the surface of the cortex (ECoG), or in a non-invasive method by placing the electrodes on the scalp (Electroencephalography - EEG). The physical characteristics of neuronal signals obtained by these measuring methods depend on the electrical mechanisms of neuronal activity. Identifying these mechanisms is essential for understanding neuronal signals' origin and functionality.

Electric fields generated by an active neuron can be modelled as the electric field of a dipole: A positive and a negative charge (poles) that are kept separate by a certain distance, thus generating an electric field in that space. This model can then be applied to an excited postsynaptic neuron. When a neuron displays a postsynaptic potential in its apical dendrites, the resulting intracellular influx of positive ions causes the local extracellular region to have an excess of negative charges (negative pole) in comparison to the extracellular space of the rest of the neuron (positive pole). Hence, postsynaptic potentials cause neurons to act as a dipole, thus inducing an electric field (Jackson & Bolger, 2014). Likewise, postsynaptic inhibitory potentials would cause an extracellular outflux of intracellular positive ions, resulting in a dipole with an opposite alignment of positive and negative charges (Jackson & Bolger, 2014).

The summation of the electric fields generated by the synchronous activation of several cortical neurons can be measured by the potential difference on electrodes placed on one's scalp, which is the principle of EEG. Essentially for EEG, an electrode is attached on the scalp surface to detect changes of the extracellular electric potential with reference to the electric potential of another predefined electrode (reference electrode). The detected electric potential by the

scalp electrode is also sensitive to the distance and orientation between the electrode and the neuronal dipole, as well as to the conductivity properties of the skull and scalp layers (Fig. 1).

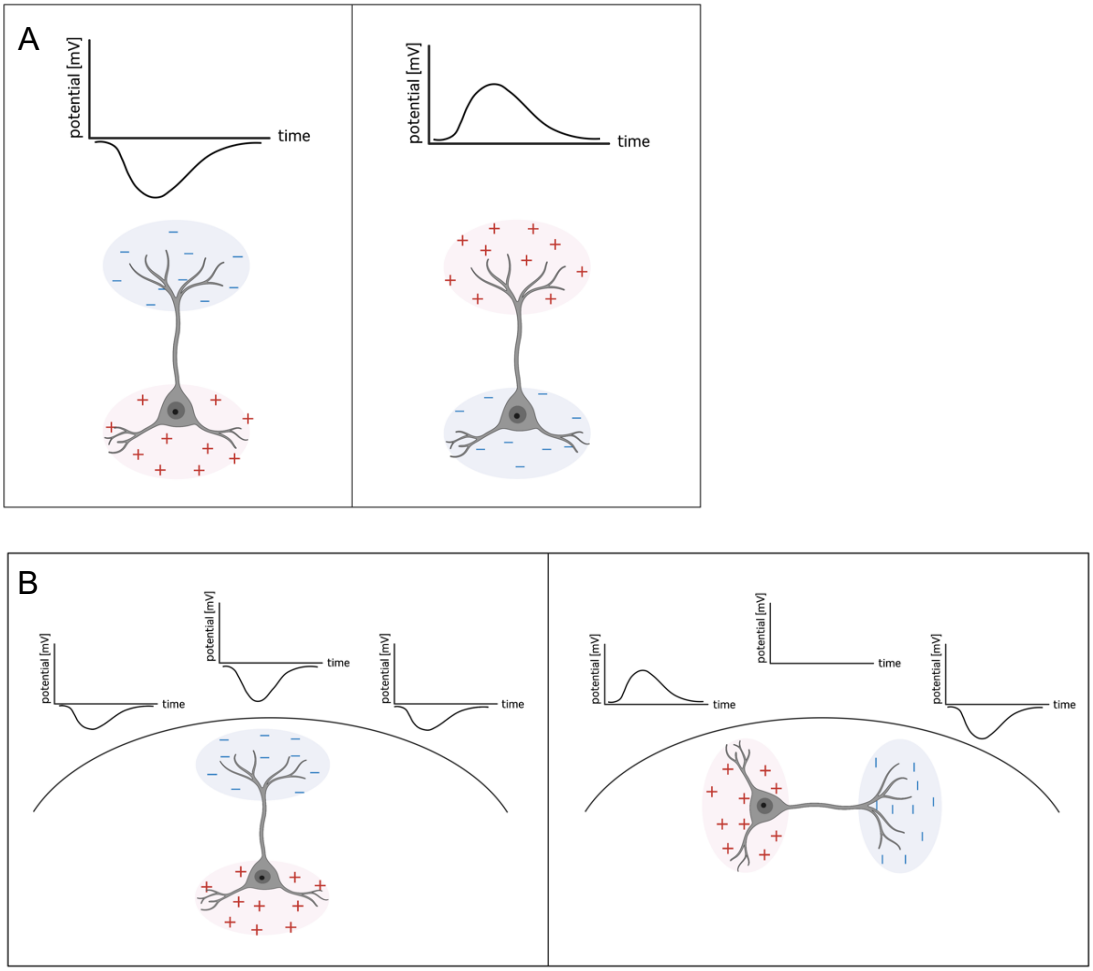

Figure 1. Examples to illustrate behavior of the electric voltage signal with regard to neuronal activity, picked up by electrodes placed on the scalp

A: Dipole orientation of a neuron affects direction of the deflection in the measured signal. Left: This neuron is facing the electrode with its negatively charged part. A negative deflection of the signal can be observed. This dipole orientation can either result from an excitatory postsynaptic potential (EPSP) at the apical dendrites or an inhibitory postsynaptic potential (IPSP) near the soma. Right: This neuron is facing the electrode with its positively charged part. A positive deflection of the signal can be observed. This dipole orientation can either result from an IPSP at the apical dendrites or an EPSP near the soma. Based on Jackson and Bolger (2014). Created with BioRender.com.

B: Relative position and orientation of the electrodes towards the neuron affect size and direction of the deflection in the measured signal. Left: Electrode closest to the electric source shows the greatest signal deflection. Deflection size decreases with increasing distance between electrode and electric source. Right: Electrodes pick up the sum of charges in their vicinity. An electrode that is equidistantly placed between a positive and negative charge shows no deflection in its signal. Based on Jackson and Bolger (2014). Created with BioRender.com.

Importantly, the potential differences measured by extracellular electrodes do not reflect the activity of a single neuron, but the sum of electric fields created by numerous neurons in its proximity. It follows that invasive local field potential (LFP) measurements detect the summarized activity of hundreds to thousands of neurons in their surroundings (Buzsaki et al., 2012), while electrocorticography (ECoG) records the activity of about half a million of neurons (Meshulam et al., 2013; Ojemann et al., 2013). EEG, however, measures the electric current generated by 30-500 millions of neurons (Nunez, 1996). It follows that EEG signals have a considerably lower spatial resolution compared to invasive methods. Scalp recordings with EEG also have the constraint that the electric field is drastically weakened by skull and scalp tissues, further compromising the identification of the neuronal sources of the reported activity. On the other hand, EEG has the clear advantage of being a non-invasive procedure that can be safely performed in any individual. Moreover, despite the poor spatial resolution, EEG can detect changes in electric potentials in the order of milliseconds, an excellent time resolution which is imperative to identify neuronal oscillatory patterns (Gevins et al., 1999).

Due to oscillating membrane potentials, rhythmic firing rates of action potentials and consequent postsynaptic potentials, neuronal circuits and even single neurons are endowed with oscillating and resonating features (Hutcheon & Yarom, 2000; Llinas, 1988). Intracellular recordings of single neurons show that they can oscillate at multiple frequencies, which suggests that the timing of their activity is relevant for information transfer within a neuronal network (Buzsaki & Draguhn, 2004). Larger neuronal populations and circuits also display oscillatory features and the sum of their synchronized activity gives rise to the electric signal that can be measured with EEG (Jackson & Bolger, 2014).

EEG signals are rarely composed of one distinct oscillation band, most of them represent a superposition of various oscillatory patterns originating from neuronal populations across the brain. These oscillatory patterns are not simply a by-product of the electric activity of neurons, but instead are functionally relevant for information processing within and among brain regions, as neuronal oscillations were found to modulate neuronal activity between brain networks (Buzsaki &

Draguhn, 2004). Neuronal oscillation patterns are classified in accordance to their frequency bands, which are found to be associated with different brain states (Fig. 2).

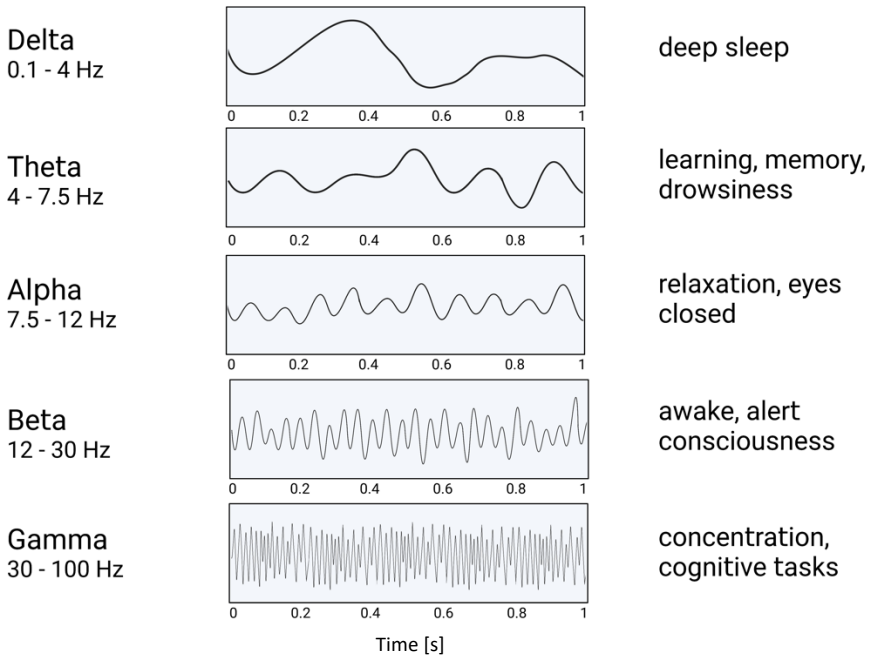

Figure 2. Classification of brain waves.

Brain oscillations can be classified according to their frequency band. Created with BioRender.com.

1.2 Communication through coherence

Various stimuli inputs from presynaptic knobs arrive at a postsynaptic neuron, generating postsynaptic potentials. If the sum of these postsynaptic potentials exceeds a threshold, an action potential is triggered in the postsynaptic neuron, thereby causing a postsynaptic potential in the downstream connected neurons. Thus, the likelihood of a neuron to fire an action potential, its sensitivity and responsivity, is based on its constantly changing membrane potential.

Accordingly, incoming timely convergent inputs from presynaptic neurons are more likely to result in an action potential than randomly timed postsynaptic potentials, which is the base of a more efficient integration and transfer of information (Buzsaki & Draguhn, 2004). This means that the arrival of timely

convergent presynaptic inputs at postsynaptic neurons in a focused manner and in coordinated time windows is more likely to result in an action potential and sending downstream information, as is the case for neuronal activation in synchrony to an oscillatory pattern. On the other hand, inputs arriving at random or in uncoordinated manner will less likely result in an action potential, thus filtering out the information (Klausberger et al., 2004).

The theory of communication through coherence (Fries, 2015) proposes that this temporal coordination underlies the synchronization of neuronal oscillations, which in turn modulates information transfer and processing in neuronal networks. For instance, when a stimulus input is selected by attention, therefore being assigned greater relevance, more pronounced oscillatory synchronization is observed in the cortical representations of the stimulus. Synchronized oscillations of activated neuronal groups entrain specific postsynaptic neurons and rhythmically link the timing of synaptic inputs to the timing of spike outputs. The changing neuronal responsivity based on the membrane potential creates repeating time windows of differing excitability between the pre- and postsynaptic neurons. While meaningful inputs arrive at states of high excitability (and are thus synchronized), noisy inputs arrive at states of low or random excitability and are thus filtered out. Therefore, only the neuronal circuitry transmitting the information of the relevant stimulus will successfully carry the information forward (Fries, 2015).

These time windows of the neuronal excitability cycle are related to the phases of synchronized neuronal oscillations in specific frequency bands, which are detectable in EEG (Fries, 2015).

1.3 Working memory and the frontoparietal network

Working memory (WM) is a cognitive function described as the capacity for temporary storage and manipulation of sensory information. Despite its seemingly basic function, it is considered to be fundamental for higher order executive functions, enabling comprehension, reasoning, learning and decision making. The concept of WM can be represented by the storage of information

(items) in the consciousness, including letters, words, numbers and objects, which are held for a couple of seconds until utilization, before they fade. This appears to contrast with long-term memory (LTM), which involves the retention of information for long periods of time, which can be retrieved under specific contingencies. This means that WM has fundamentally different functions and neural underpinnings from LTM (Cowan, 2014). Moreover, WM is considered to include two functions: the temporal storage of internal representations of stimuli and further processing operations that are performed on these representations (Curtis & D'Esposito, 2003). The temporal storage of internal representations is thought to involve the placement of neuronal circuits containing information in a state of higher responsivity, allowing its immediate retrieval. The function of processing operations enables the manipulation of that stored information, and it is thought to involve interfaces with other cognitive functions (Curtis & D'Esposito, 2003).

The neuronal structure and function of the WM system is complex and so far, not fully understood. One of the most common models of WM is the multicomponent model introduced by Baddeley (1992). It proposes the idea that WM consists of two short-term memory (STM) buffers, namely the verbal (“phonological loop”) and the visuospatial (“visuospatial sketchpad”) STM buffer. Both buffers work independently from each other, and are directed by an attentional controlling system, named the “central executive”.

Later, state-based models of WM have gained in importance. According to these, the functioning of STM is based on the allocation of attention to internal representations of items in WM. That is, WM items are maintained in one of several activation states by the allocation of attention, thus becoming accessible for cognitive processing (Cowan, 1995; D'Esposito & Postle, 2015). Similar to the phonological loop and the visuospatial sketchpad of the multicomponent model, state-based models also can be divided into activated LTM models and sensorimotor recruitment models. The activated LTM model is associated with semantic stimuli (digits, letters, words), whereas the sensorimotor recruitment model is associated with perceptual stimuli (visual colors and shapes, auditory pitches) (D'Esposito & Postle, 2015).

It is well known that cognitive tasks involving verbal stimuli primarily tend to activate left hemispheric brain areas, while visuospatial tasks are linked to the activation of the right hemisphere (Clark et al., 2001; Smith et al., 1996).

In neuroimaging studies, prefrontal and parietal regions of human subjects exhibited a higher activity during their engagement in a WM task, suggesting their functional relevance for WM (Cabeza & Nyberg, 1997; Courtney et al., 1998; Manoach et al., 1997). The prefrontal cortex (PFC) is involved in higher cognitive functions of the brain and it is associated with cognitive control, which results in the capacity to direct thoughts and actions in accordance with internal goals. This is essential for reasoning, planning and ultimately WM (Goldman-Rakic, 1987; Jimura et al., 2018; Kim et al., 2015; Miller & Cohen, 2001). During the retention period of delayed WM response tasks, in which external stimuli are absent, the PFC exhibits persistent activity (Courtney et al., 1997; Fuster & Alexander, 1971). The neuronal activity in the PFC also serves as a predictor for the retrieval accuracy in WM tasks, further suggesting its functional importance for WM (Melrose et al., 2020).

Another important cortical region for WM is the posterior parietal cortex (PPC), located between the somatosensory and visual cortex, which is proposed to have an associative role by integrating inputs from different brain regions including the somatosensory, auditory, visual, motor and prefrontal cortical regions (Culham & Kanwisher, 2001; Whitlock, 2017). The PPC is shown to be relevant for visuomotor control, spatial perception and attention (Andersen, 1997; Jackson & Husain, 2006; Malhotra et al., 2009). The strong structural and functional connectivity between the PFC and the PPC seen in both rodents and humans suggested the conceptualization of the frontoparietal network (FPN), which is involved in executive functions, including working memory (Deserno et al., 2012; Friedman & Goldman-Rakic, 1994; Olesen et al., 2004; Sauseng et al., 2005).

In the FPN, the interaction between attention allocation and sensory stimuli allows selection of relevant stimuli, which is controlled by knowledge, expectation and goals, meaning that it serves as an executive system (Osaka et al., 2004). The allocation of attention in decision-making is necessary due to the continuous

exposure to an abundance of stimuli, many of which are not particularly relevant to the goal behavior (Corbetta, 1998; Corbetta & Shulman, 2002). The interaction between the PFC and the PPC in the FPN is described as a top-down control mechanism (D'Esposito et al., 2000; Miller & Cohen, 2001). That is, for the maintenance of items in WM, the attention allocation performed by the PFC acts by selecting internal representations of relevant stimuli, which are stored in posterior regions of the brain (Buschman & Miller, 2007; Curtis & D'Esposito, 2003).

1.4 Frontal-midline theta oscillations

The relevance of theta oscillations in cognitive performances has been thoroughly described in rodent hippocampus. Hippocampal theta activity and its rhythmicity are involved in cognitive functions including learning and memory. For instance, while exploring a maze, rats show an increased firing rate of hippocampal neurons and a coherence of the firing rate to the ongoing theta rhythm (Buzsáki & Moser, 2013; Jensen & Lisman, 2000). Apart from the hippocampal formation, theta oscillations are also observed in the activity of several other cortical structures, including the entorhinal cortex, cingulate cortex (Feenstra & Holsheimer, 1979), posterior (Colom et al., 1988) and prefrontal areas (Siapas et al., 2005) in rodents.

In humans, theta oscillations are distributed across brain networks and can be detected in frontal cortical regions via EEG, i.e., theta oscillations from the frontal midline of the brain (Raghavachari et al., 2001). Frontal-midline theta (FM theta) oscillations exhibit bouts of oscillatory synchrony with the hippocampal rhythmicity, thus suggesting their functional significance in cognition, including memory retention and attentional processes (Gevins et al., 1998; Ishii et al., 1999; Mitchell et al., 2008; Young & McNaughton, 2009). FM theta oscillations are observed in different types of memory tasks, with higher memory load and task difficulty leading to increased amplitudes of the theta oscillation (Jensen & Tesche, 2002; Sauseng et al., 2007). Furthermore, frontal-theta can be observed especially during periods of encoding, retention and retrieval, further suggesting that FM theta is functionally relevant for WM (Mitchell et al., 2008).

As mentioned, theta oscillation is not locally limited to the frontal cortex. Coherent neuronal activity in the theta band can be detected between prefrontal and temporo-parietal areas during WM retention of verbal and visuospatial items. Interregional synchronization of theta oscillations is proposed to integrate cortical areas in the circuit of WM. During the retention of verbal items, the brain exhibits strong theta synchronization between prefrontal and left temporo-parietal areas, whereas strong frontoparietal synchronization in the right hemisphere can be observed during the retention of visuospatial items (Sarnthein et al., 1998).

The strong synchronization of theta oscillations between cortical hubs of the FPN during WM task activity suggests that the oscillatory activity in this specific band frequency modulates WM processing. The theta rhythm might reflect a gating mechanism, which processes task-relevant information and suppresses task-irrelevant information (Sauseng et al., 2010). In this framework, phases of the theta rhythm reflect different states of excitability, in which neurons encoding relevant information are firing precisely in synchrony to that oscillation during the high excitability phases, and are thus able to modulate information and transmit it downstream (Cavanagh & Frank, 2014).

Besides FM-theta oscillations, gamma oscillations (30-100 Hz) in the temporo-parietal cortex are also strongly associated with WM processing (Lutzenberger et al., 2002; Morgan et al., 2011). Gamma oscillations are commonly observed in neocortical, entorhinal, hippocampal and many other areas (Buzsaki & Wang, 2012). Gamma oscillations can be described with several models. One of them is the E/I (excitation/inhibition) model, which is based on the functional connection between pools of excitatory pyramidal and inhibitory neurons, with the latter regulating the activity of the excitatory projection neurons, thus maintaining a balance between excitatory and inhibitory inputs. The spiking of pyramidal cells and the delayed spiking of interneurons alternate, giving rise to the fast oscillatory activity in the gamma band (Buzsaki & Wang, 2012; Mueller-Buehl et al., 2023).

During cognitive tasks, theta and gamma oscillations frequently occur together (Bragin et al., 1995; Lasztoczi & Klausberger, 2014). Fast oscillations like gamma occur locally, whereas slow oscillations can entrain more neurons in a wider

range and are associated with larger membrane potentials, which is why their synchronized activity can be observed across neuronal networks (Buzsaki & Wang, 2012; von Stein & Sarnthein, 2000). In order to transfer information among cortical areas of larger distance, it has been shown that gamma oscillations can be modulated by prefrontal theta oscillations (Buzsaki & Wang, 2012). Gamma and theta oscillations are synchronized via cross-frequency coupling, which has been observed both in rodents and humans (Berger et al., 2019; Penttonen et al., 1998). That is, posterior gamma oscillations are nested into specific phases of theta oscillations of the prefrontal cortex during processes of WM (Belluscio et al., 2012; Penttonen et al., 1998; Siegel et al., 2009). The strength of this phase-coupling appears to be a predictive indicator for the accuracy of memory performance (Axmacher et al., 2010; Lisman & Jensen, 2013).

Temporo-parietal gamma oscillations are noted to be nested in the trough of the prefrontal theta oscillation in cognitively demanding tasks, whereas they are nested in the peak during easier cognitive tasks (Fig. 3) (Berger et al., 2019). This suggests that the trough of FM theta might represent a state of high excitability, whereas the peak of FM theta might represent a state of low excitability in the WM circuit. Difficult tasks require more cognitive resources that can be more easily recruited during high excitability states.

Neuronal spiking in the parietal cortex is then temporally aligned with neuronal spiking of the prefrontal cortex, thus allowing stronger coupling of the FPN. Tasks of low cognitive demand however do not require strong coupling of the FPN, thus leading to non-simultaneous firing.

Therefore, it is assumed that the phase of FM theta oscillations can modulate gamma oscillations, thus enabling coupling and decoupling of the frontoparietal WM circuit in humans (Berger et al., 2019).

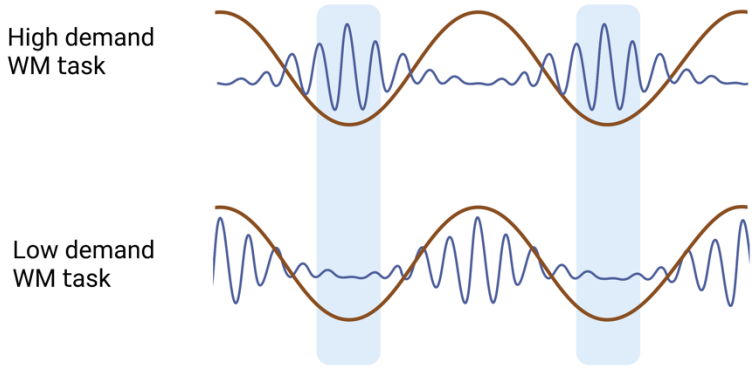

Figure 3. Power-phase coupling of theta and gamma oscillations during WM tasks of different cognitive demand.

Amplitude of gamma oscillations in the parietal cortex (blue) is modulated by the phase of the ongoing theta oscillation in the prefrontal cortex (brown). Depending on the difficulty of the WM task, gamma oscillations are either preferably nested in the trough (phase of low excitability) or trough (phase of high excitability) of the theta oscillation. Based on Berger et al. (2019). Created with BioRender.com.

1.5 Transcranial magnetic stimulation

Transcranial magnetic stimulation (TMS) is a non-invasive method of brain stimulation which can safely depolarize neuronal populations located in superficial cortical areas (Hallett, 2007).

For stimulation, the TMS coil is placed on a subject's head. A pulse of electrical current passes through the wired coil and induces a short-term magnetic field perpendicular to the plane of the coil (Fig. 4A). This magnetic field can reach a strength of about 2T and can last for 100μs (Hallett, 2007). The change of the magnetic field induces an electric field in the cortex perpendicular to the magnetic field. While the strength of the magnetic field is proportional to the electric current through the coil, the strength of the electric field induced in the brain is proportional to the rate of change of the magnetic field. This electric field depolarizes neurons, causing physiological and behavioral effects depending on the targeted brain area.

For instance, if TMS is applied on the motor cortex on one hemisphere with enough stimulation intensity, motor evoked potentials (MEPs) can be recorded from the contralateral extremity muscles. This stimulation intensity required to elicit MEPs has an inter- and intraindividual variability, suggesting that other

cortical areas also have a variable stimulation threshold. So, for comparing TMS data it is necessary to set a benchmark for the stimulation intensity, as different intensities trigger outcomes of differing size. The objective measurement of MEPs is frequently used for quantifying the TMS stimulation intensity. It can be used to indicate membrane excitability of corticospinal neurons and also other cortical neurons (Kobayashi & Pascual-Leone, 2003).

With a figure of eight coil, TMS can depolarize neurons up to approximately 2cm below the scalp, sufficient to stimulate superficial areas in a very spatially focal manner (Fig. 4B) (Galhardoni et al., 2015).

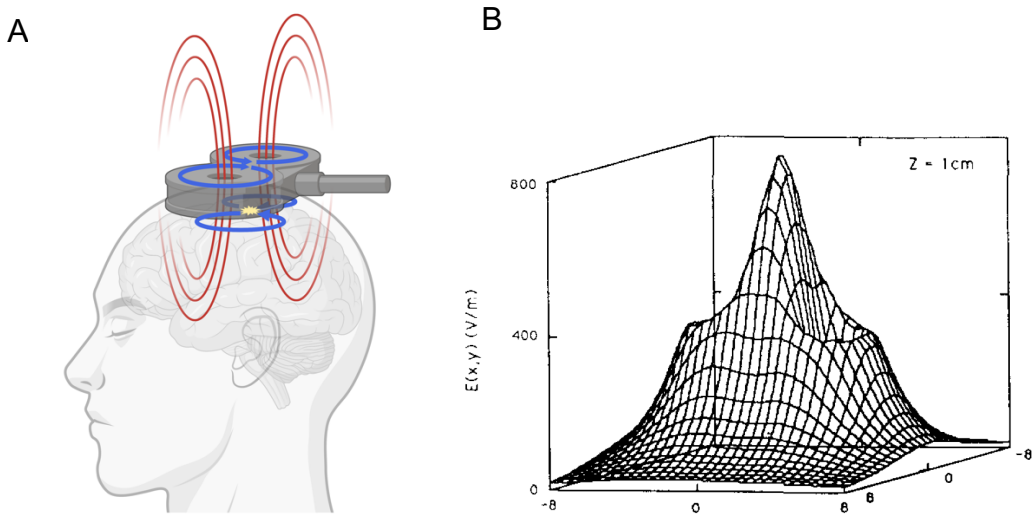

Figure 4. Physical functioning of TMS.

A: A coil is placed on a subject's head. A brief current pulse is sent through the wired coil (blue). A flowing current induces a magnetic field (red). Changes of power or direction of the induced magnetic field induce a perpendicular electric field in the brain (blue). The electric field causes currents among neuronal groups. Created with BioRender.com.

B: Extracted from Cohen et al. (1990). Every coil shape results in a different morphology of the induced electric fields. If using a figure-of-eight coil, the strength of the electric field is focused in one particular point, thus allowing precise stimulation with a figure-of-eight coil.

TMS pulses applied to cortical regions other than the primary motor cortex also result in clinically relevant effects. For instance, delivering TMS pulses to cortical regions associated with language lead to speech disruption (Tarapore et al.,

2013). So, TMS can be used for testing the excitability of cortical regions and cortical functional mapping, as part of the planning for neurosurgical procedures (Hallett, 2007). This includes presurgical mapping of speech, language and motor skills with the attempt to minimize resulting postsurgical functional deficits (Narayana et al., 2021).

Similar to the disruption of speech, TMS can be also used for the disruption of other cognitive systems. In 2019, Berger et al. investigated the effect of TMS on WM performance in humans. Their experiment showed that TMS triple pulses (50Hz, i.e., 2ms between consecutive pulses in the triplet) at the right posterior parietal cortex (PPC) can disrupt working memory retention. Importantly, this happened for trials, in which the pulses were delivered during the trough of the prefrontal theta oscillation. This observation was possible by analyzing the EEG recorded during the stimulation and estimating the phase of the theta oscillation during which each pulse was applied, in a post hoc manner (Berger et al., 2019).

1.6 Brain state-dependent EEG-TMS

As phases of an ongoing neuronal oscillation represent specific excitability states of the brain, the timing of delivering a TMS pulse becomes an important parameter, affecting behavioral and physiological outcomes differently.

In fact, when applying TMS on cortical areas with the same paradigm on the same individual for instance, there is still a substantial variability in the responsive outcomes (Lopez-Alonso et al., 2014; Muller-Dahlhaus et al., 2008). This is because the brain rapidly undergoes changing brain states, which are entrained by neuronal oscillations and which modulate the outcome. With the attempt to deliver TMS pulses precisely to a predefined phase of a given oscillation, the method of brain state-dependent EEG-TMS has emerged recently and has increasingly gained traction in the TMS field of research.

With the method of brain state-dependent EEG-TMS, it has been demonstrated that targeting the trough of the mu-rhythm (7-11Hz over the sensorimotor cortex),

when stimulating the primary motor cortex, evoked higher motor evoked potentials than TMS targeted at the peak of the mu-oscillation (Zrenner et al., 2018).

The same principle can be further extended onto other physiological brain oscillations, namely prefrontal theta oscillations.

It has also been shown with the same method that targeting the prefrontal theta oscillation at its higher excitability state, namely the trough of the theta oscillation, led to an enhanced cortical responsivity in the theta oscillation band and shorter response times for correctly answered trials in WM tasks (Gordon et al., 2022; Gordon et al., 2021).

1.7 Study objective and hypothesis

This study aims to investigate the possibility of modulating WM of healthy human subjects in real-time, using brain state-dependent EEG-TMS with stimuli phase-locked to theta oscillations of the prefrontal cortex.

This study aims to reproduce these results by Berger et al., (2019), but also go further by making use of a brain state-dependent stimulation paradigm to specifically target the trough of prefrontal theta oscillations during the execution of a WM task in real-time. The specific targets of stimulation are the right posterior parietal cortex (PPC) and the left dorsomedial prefrontal cortex (DMPFC). In the case of the PPC, we expect an impairment of WM, since stimulation in a high excitability state, namely the trough of theta oscillations in the prefrontal cortex, would cause a strong interference in the parietal cortex, which holds representations of memory items.

Other than impairing WM, it also would be desirable to be able to facilitate memory retrieval. We propose that, instead of disrupting the PPC with TMS, theta phase-locked TMS to the prefrontal cortex will facilitate top-down input from the prefrontal cortex to parietal cortex through the frontal-parietal WM network, thus increasing the likelihood of memory retention.

2 Materials and Methods

2.1 Participants

Inclusion criteria were age between 18 and 50 years, absence of current or former neurological and psychiatric disease and competence to consent to participate in the study. Exclusion criteria included current treatment with central nervous system active drugs, illicit drug abuse, head injury, MRI incompatibility (presence of metallic or electronic medical implants, e.g., cardiac pace-maker) and resting motor threshold (RMT) >70%.

All subjects provided written consent prior to participation. The study was conducted in accordance with the Declaration of Helsinki and approved by the local ethics committee, Faculty of Medicine of the Eberhard-Karls-University, Tübingen (536/2020B).

A total of 21 participants aged between 21 and 38 years were recruited for the 2-sessions experiment. Of the 21 participants one was excluded due to too high RMT. The final sample included 20 participants (11 female) with a mean age of 25 $\pm$ 5 years (SD). Twenty subjects participated in session A. In total, fourteen subjects participated in session B, as six subjects did not tolerate the stimulation session due to discomfort or pain.

2.2 Main Experiment

2.2.1 Experimental protocol

During the experimental sessions subjects were sitting comfortably in a reclined chair in front of a monitor screen and were instructed to relax while executing the memory tasks of the experiment.

The study comprised 2 sessions (session A and session B) performed on different days (at least 2 days apart). Each of the sessions followed the same protocol with the same methods, but had different cortical targets for the application of TMS (Fig. 6). The cortical targets were the right posterior parietal cortex (PPC) for

session A and the dorsomedial prefrontal cortex (DMPFC) for session B. The order in which the sessions were applied was randomized for each subject.

Each session included the following steps: 1) 8 min of EEG recording during the execution of a WM task, 2) 20 min EEG recording during the execution of a WM task with the phase-detection algorithm on, marking the EEG when the TMS pulses would be applied, but without real stimulation, 3) 6 blocks of phase-specific TMS application during WM task execution.

The first recording (Fig. 6, A) was used for the computation of the covariance matrix, which was required for the individualized spatial filter w. The spatial filter w was used for the estimation of the source activity of the prefrontal theta oscillation. The data acquired from the first recording was also used to estimate the SNR of theta oscillations and optimize the parameters for the spatial filter. EEG was recorded while the subject was engaged in memory tasks, aiming to increase the power of the theta band oscillation. The relevance and details of extracting the theta phase will be discussed below.

For the phase specific TMS application, we used the algorithm for real-time phase estimation developed by Zrenner et al. (2020). The method involves band-pass filtering the raw real-time EEG signal with respect to the frequency of interest. The edges of the signal, which contain the filtering artifact, are then clipped out. In order to obtain an estimate of the signal at real-time, the signal is then reconstructed using a forward-predictive model. The phase of the signal at real-time is then estimated using the Hilbert transform. If the estimated phase corresponds to the phase of interest, a trigger signal is then sent to the TMS device (Fig. 5).

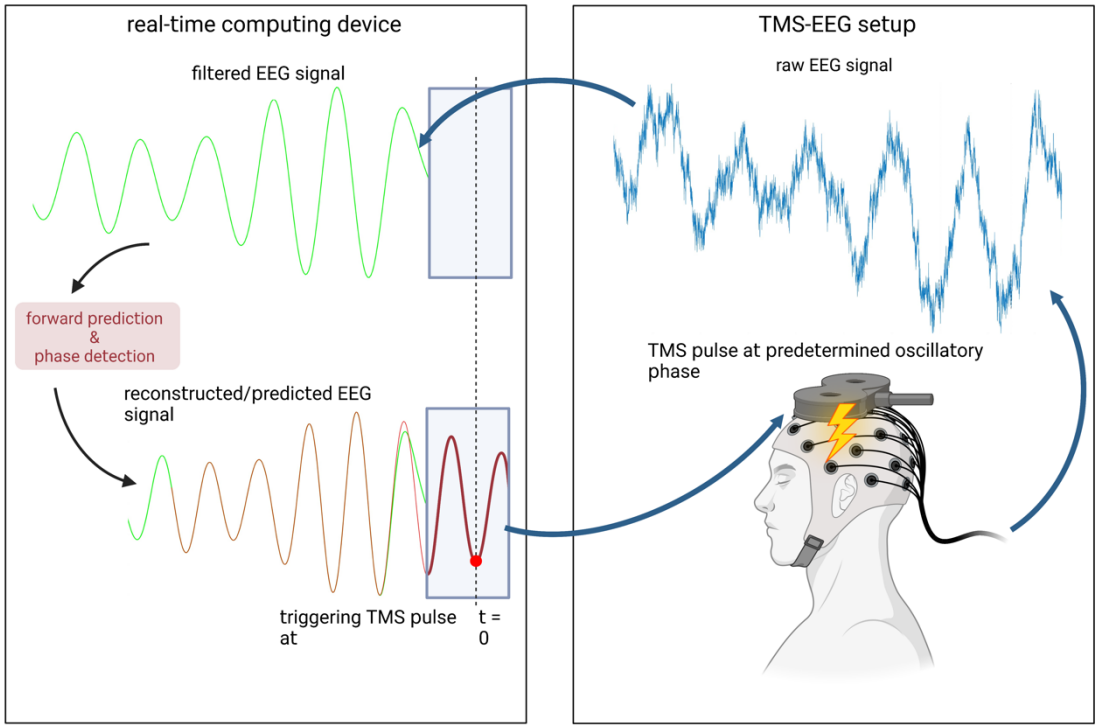

Figure 5. Methodological principle of brain state-dependent EEG-TMS.

The raw EEG-signal is band-pass filtered to extract the theta frequency band of interest. An EEG signal is then reconstructed and then predicted, based on the EEG signal in the preceding time window. A TMS pulse is triggered at the phase of interest (time = 0) of the predicted signal. Created with BioRender.com.

The second recording (Fig. 6, B) was necessary to quantify the accuracy of the algorithm predicting the phases of theta oscillations. For this purpose, real-time markers were set during the EEG recording, whenever the conditions for triggering at the trough or uncoupled to the ongoing theta oscillation were met. The markers in the EEG data were evaluated post-hoc to estimate the phase accuracy. This post-hoc phase estimation uses pre- and unperturbed "post-stimulus" EEG data signal to determine the theta phase during which the trigger was sent. This feature allows the use of longer epochs of data and a higher filter order, in addition to not needing to rely on a forward predicted signal, making it the gold standard for the actual theta phase, against which the estimated phase from the real-time algorithm is compared. This verification of the phase accuracy can only be done on EEG data without TMS. TMS pulses considerably distort the data after the stimulus, hindering the post-hoc phase estimation due to the

presence of TMS-triggering electrical artifacts, as well as subsequent muscle contractions and sensory evoked potentials, thus making any phase estimation in the presence of TMS delivery unreliable.

Since the phase estimation uses the same procedure in recording sequences with and without TMS of each session, this method serves as a reliable indicator for the quality and accuracy of the phase estimation in the stimulation blocks.

In the third part of the experiment (Fig. 6, C) all subjects underwent six blocks of WM tasks of two alternating types, namely a Sternberg task and a visuospatial memory task, with concomitant TMS application. A training block was carried out before the real experiment. The Sternberg memory task blocks included 140 trials. The visuospatial WM task block included 260 trials, 130 trials each for the identical and mirrored visuospatial memory task type. Subjects could relax during short breaks of 5 minutes between the task blocks. Figures 7 and 8 display the course of the tasks.

Each task block involved the delivery of phase specific TMS pulses, 1 TMS pulse per WM task trial. TMS pulses were applied in accordance to 4 different conditions, which were randomized among trials: 1) sham/trough, 2) active/through, 3) sham/random phase and 4) active/random phase.

In active condition trials, a set of three biphasic TMS pulses (f = 100Hz) with an intensity of 120% RMT was applied to the cortical target during either the trough or at random phase of the prefrontal theta band. A direct contact between the coil and scalp was avoided due to resulting electric artefacts introduced by TMS. Instead, a gap of 6 mm was maintained by using a coil spacer made of plastic (Ruddy et al., 2018).

In sham trials, no TMS was delivered to the subject’s head. In place of TMS, electrical stimulation was applied to the subject via electrodes placed on the scalp. The intensity used was individually adjusted to the sensation of the TMS pulse, so that it caused a significantly stronger somatosensory input as the TMS only. This was done to make the sensory input between the sham and real TMS application comparable, as explained in a further section.

In each trial, TMS and/or electrical pulses were delivered after the offset of the memory set during the retention period in the memory task in the active condition.

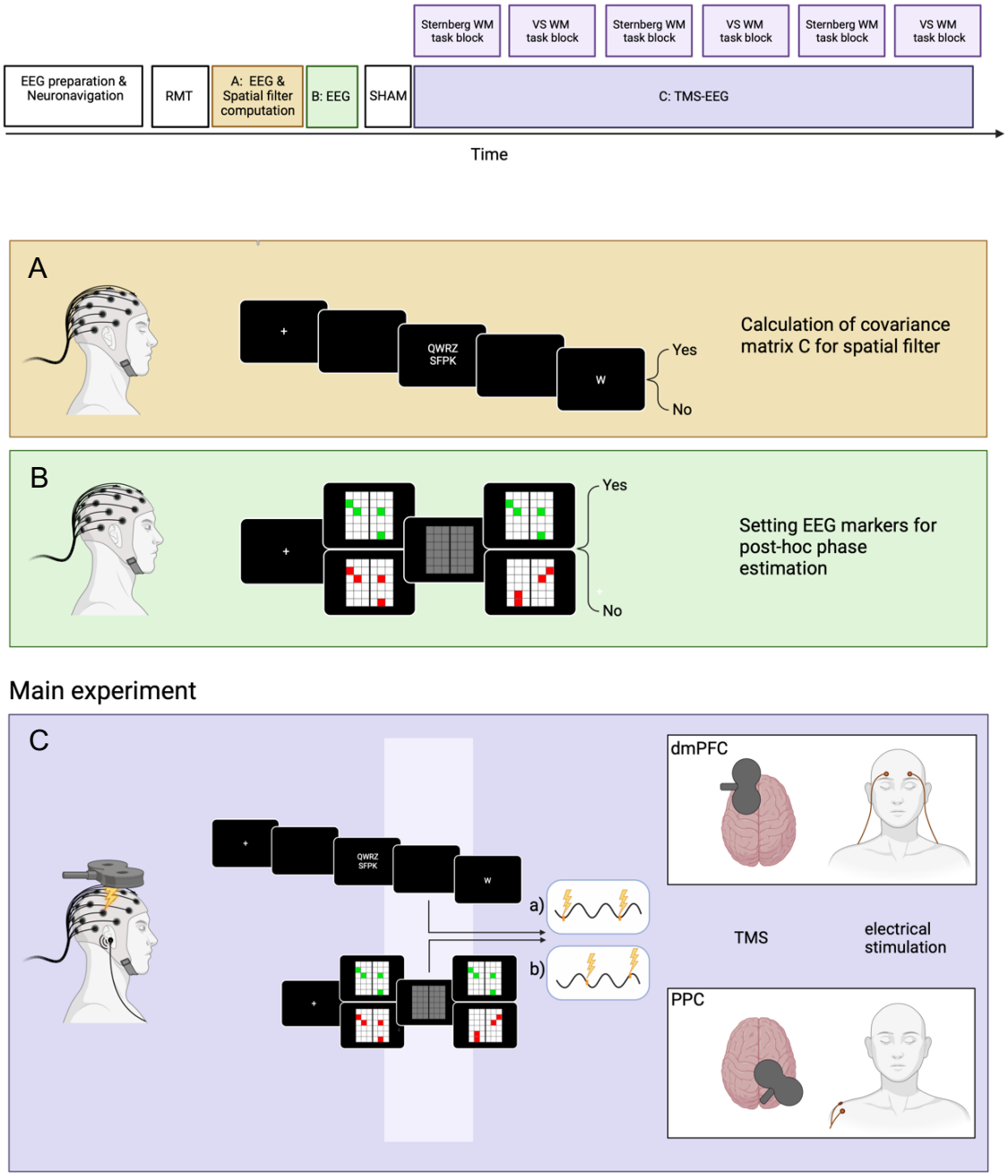

Figure 6. Timeline and outline of the experimental session.

Exemplary timeline of one experimental session: Blocks in color (A: yellow, B: green, C: purple) indicate measurements. Blocks in white indicate preparatory steps.

A: EEG recording during a WM task for the computation of the individualized spatial filter w.

B: EEG recording with marker setting during WM task by using the real-time paradigm for the post-hoc phase estimation.

C: TMS and electric stimulation were applied either at the trough (a) or uncoupled (b) of the ongoing theta oscillation during the retention period of WM tasks by using the real-time paradigm. Created with BioRender.com.

2.2.2 Working memory tasks

We used the Sternberg memory task and the visuospatial WM task, which are two different types of WM tasks that involve different cortical regions for storing and processing WM items. The visuospatial task was adapted from Berger et al., (2019). Berger et al., (2019) observed high connectivity between prefrontal theta and right temporo-parietal gamma oscillations during visuospatial memory activity, thus highlighting the role of the right hemispheric regions for visuospatial tasks, as also previously shown by other PET and fMRI studies (D'Esposito et al., 1998; Jonides et al., 1993). For verbal tasks, as is the case of the Sternberg task, the brain activity exhibits a lateralization to the left hemisphere (Wager & Smith, 2003). In order to further investigate the impact of the same stimulation protocol on another functional memory circuit, the verbal Sternberg task was also included in the experiment in addition to the visuospatial task.

2.2.2.1 Sternberg memory task

Sternberg designed this task to investigate cognitive processing and short-term memory and could conclude a linear correlation between the number of items and reaction time (Sternberg, 1966, 1969). The Sternberg memory task has since become a very popular method in cognitive and experimental psychology (Roznowski & Smith, 1993).

A sequence of eight randomized consonant letters is presented on the screen of the display toolbox (VIEWPixx, VPixx Technologies Inc., Canada) in front of the subject (Fig. 7). It is followed by a retention period, during which the screen turns blank. Subjects are instructed to retain the presented items in this period, until a random probe letter is presented. Subjects then have to decide whether the probe letter was part of the memory set or not by pressing the corresponding buttons

“Yes” or “No” on a handheld response box (RESPONSEPixx Handheld, VPixx Technologies Inc., Canada) as fast as possible. For each trial, the response accuracy and response time were logged by the display toolbox.

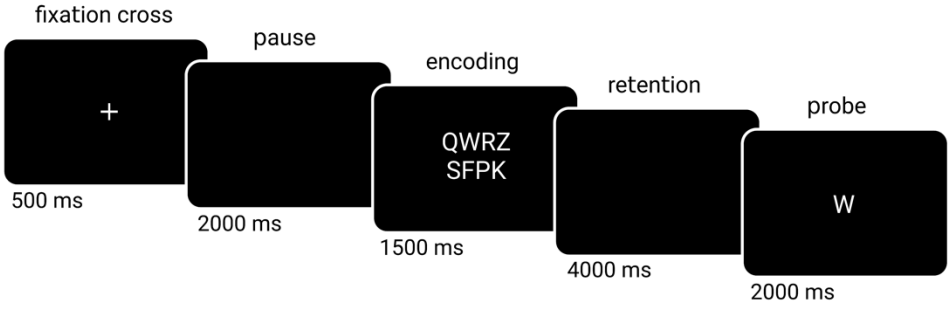

Figure 7. Design of the Sternberg WM task.

In the encoding period, a sequence of eight randomized consonants was presented on the screen. Subjects were instructed to retain the consonants for a period of time until a probe letter was presented. Subjects were instructed to press corresponding buttons on a response box, whether the probe letter was part of the memory set or not. Created with BioRender.com.

2.2.2.2 Visuospatial memory task

In the visuospatial memory task, a 6x6 grid display is presented on the monitor screen in front of the subject (Fig. 8). Four squares in randomized grid positions are all colored uniformly either in green or red. The square color indicates the memory task type: If the squares are colored green, their identical positions in the grid are supposed to be retained. If the squares are red, their respective positions have to be vertically mirrored on the highlighted midline of the grid and then retained during the retention period. After the retention period, a probe grid is presented. Depending on the square color in the encoding period, subjects have to decide whether the grid shows the correct identical or mirrored positions of the colored squares by pressing the corresponding buttons “Yes” or “No” on a handheld response box (RESPONSEPixx Handheld, VPixx Technologies Inc., Canada). For each trial, the response accuracy and response time were logged by the display toolbox.

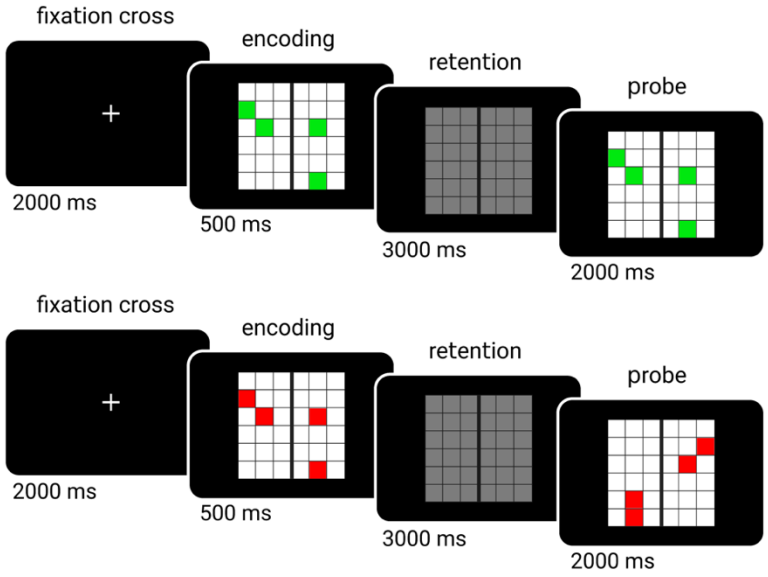

Figure 8. Design of the visuospatial WM task.

In the encoding period, a grid with four colored squares of randomized position was presented on the screen. The colors of the squares indicated the type of WM task: Green indicated the identical WM task and red indicated the mirroring WM task. Depending on the color, subjects were instructed to retain the identical or mirrored positions of the colored squares for a period of time until a probe grid was presented. Subjects were instructed to press corresponding buttons on a response box, whether or not the probe grid showed the correct positions of the colored squares according to the task type. Created with BioRender.com.

2.2.3 Electrical stimulation

The delivery of a TMS pulse is accompanied by a clicking sound of the electric discharge and a local sensation on the subject's scalp. To rule out any effects of the sensory stimuli on the behavioral response (Abler et al., 2005), electrical stimulation was used in this study to create an additional sham TMS condition to the active TMS condition. The aim was to make the saliency of the sensation caused by electrical stimulation overwhelm that of the TMS pulse, thus masking the sensation of the TMS pulse for the subject

Bipolar electrodes were attached on the skin with a conductive gel (Signa gel®, Parker Laboratories, Inc., USA). To reduce artefacts, the electrodes for electrical stimulation were placed outside the EEG cap, so that the contact to the electrodes on the EEG cap was minimized as much as possible. For mimicking the sensation of the TMS pulse on the DMPFC and the PPC, the electrical electrodes were placed on locations close to the cortical target areas. In the

DMPFC session electrical electrodes were attached pairwise to the subject's forehead, below the EEG cap. In the PPC session the electrical electrodes were attached to the subject's right acromion.

During the experiment in the active TMS condition, electric double pulses (50Hz) were applied simultaneously to the triple TMS pulses in each triggered trial. In the sham condition, electric double pulses (50Hz) were applied without TMS.

The amperage of the bipolar electrical stimulation delivered by the stimulator (DS8R biphasic constant current stimulator, Digitimer Ltd. UK) was adjusted individually according to the subject's perception (pulse width t=100μs).

2.2.4 Masking noise

In order to prevent possible behavioral effects caused by auditory stimuli, the clicking sound of the TMS coil was masked. During the experiment subjects wore in-ear headphones (Sony, MDR-EX15LP), through which a masking noise was played. The masking noise was generated with the toolbox TAAC (Russo et al., 2021). This toolbox generates a masking noise as combination of white noise and the clicking noise of the coil. It allows the customization of the masking noise according to the subject's auditory perception to the TMS in order to further disrupt the subject's perception to the TMS clicking sound.

Prior to the experiment, the volume of the masking noise was adjusted manually for each subject while test pulses of the required intensity were applied. The volume was continuously increased until the subject reported not to hear the TMS clicking sound or until the masking noise volume became intolerable.

2.3 Detection and prediction of the prefrontal theta phase

Firstly, for targeting specific phases of prefrontal theta, the oscillation band needs to be extracted among other oscillations from the brain. Theta oscillations have a lower signal-to-noise ratio (SNR) than sensorimotor mu-oscillations, which have successfully been targeted in previous experiments by Zrenner et al. (2018).

Lower SNR is associated with a higher sensitivity to interference with other oscillatory sources, which consequently decreases the accuracy of phase detection (Zrenner et al., 2020).

Secondly, the functioning of phase estimation algorithms relies on clean input data over an extended time window. However, it has been shown that cortical theta oscillations occur in limited time windows, so-called bursts, consisting of a few cycles, thus making them more vulnerable to phase resets and amplitude shifts. The presence of phase-amplitude resets, amplitude variations and signal disturbances from other unrelated sources compromise the algorithm's accuracy in predicting the proper phase of the prefrontal theta oscillation (Gordon et al., 2021; Kahana et al., 1999; Rizzuto et al., 2003; Zrenner et al., 2020).

Therefore, a method to reliably extract theta oscillations from the cortical region of interest needs to be established. This will be discussed in the following sections 2.4, 2.5 and 2.6. Further, it needs to be ensured that the input signal to the real-time system is clean, free of any phase resets and amplitude shifts. This will be addressed in section 2.7.

2.4 Spatial filters and MR-imaging

The EEG signal of one single channel on the scalp surface can be traced back to multiple oscillatory sources in the brain with their signals overlapping with each other (Fig. 9), depending on the various spatial and conduction properties of head structures, including the scalp, skull, CSF (cerebrospinal fluid) and brain cortex. This so-called volume conduction renders scalp EEG signals difficult to attribute to specific sources in the brain.

Attempts to properly localize EEG sources are divided in the forward and the inverse problem. The inverse problem refers to the efforts to find the source activity responsible for the recorded EEG signal (Grech et al., 2008). However, since the number of solutions for the inverse problem is infinite, sensible constraints need to be introduced in order to find a unique solution. These constraints are given by the forward problem. A forward model assumes

hypothetical source distributions inside the head and computes the scalp potentials that would result from them (Hallez et al., 2007). For the forward problem of any given source configuration, spatial filters are used. Spatial filters (partially) address volume conduction and can be applied on EEG data for the estimation of the source activity to solve the inverse problem.

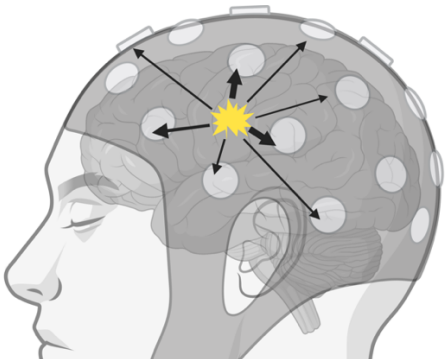

Figure 9. Illustration of volume conduction of a signal within the brain.

A single electrical source contributes to the measured signal of all neighboring electrodes. Vice versa, an electrode picks up the signal of multiple electric sources all at once. Created with BioRender.com.

A spatial filter is a weighting of signals from the individual EEG sensors. One family of commonly used spatial filters is the Surface Laplacian. The Surface Laplacian minimizes distant and deep sources in the EEG signal to attenuate volume conduction and thereby reinforces electrical activity close to the electrode. That is, as distant noise is picked up by electrodes almost equally, the average signal of the surrounding electrodes can be subtracted from the signal of the central electrode for noise reduction (Carvalhaes & de Barros, 2015). Surface Laplacians have been used successfully for the motor system (Stefanou et al., 2018; Zrenner et al., 2018). However, it is not clear *a priori*, which surface Laplacian filter should be used to target frontal theta oscillations.

An alternative proposed by Gordon, Dörre et al. 2021 involves the use of individualized filters and was shown to be more sensitive than the Surface Laplacian. For this study, an individualized source-based spatial filter was constructed and used for each subject, as already demonstrated and identically used by Gordon, Dörre et al. 2021. This proposed individualized filter for source

reconstruction requires 1) a head model, 2) a source model and 3) a sensor description.

1) The head model is supposed to set a theoretical framework for describing the behavior of electrical and magnetic fields in the head. Here, a head model with three layers, comprising the intracranial space (0.33S/m), skull (0.0041S/m), and scalp (0.33 S), was computed for each subject (Fig. 10). For the construction of the head model, we acquired anatomical T1- and T2-weighted MR images from all subjects with a Siemens Magnetom Prisma 3 T. The individual MRIs were then segmented and meshed using the Fieldtrip toolbox (Oostenveld et al., 2011), which relies on the software packages FreeSurfer and HCP workbench (Fischl, 2012). Meshes were imported into MATLAB 2018b (Mathworks Ltd., United States) and by using a customized pipeline (Nummenmaa et al., 2013; Stenroos & Sarvas, 2012) a forward model for EEG was built (Gordon et al., 2021).

2) A source model describes the position of the electric sources, which contribute to the EEG signal. For this study we used a model with approximately 16,000 cortical source dipoles, each arranged perpendicular to the cortical surface.

3) The sensor description includes the positions of the EEG electrodes on the subject's scalp, which pick up the signal from the sources. The EEG electrodes were manually registered with an MRI-guided neuronavigation system (Localite GmbH, Sankt Augustin, Germany) and then projected onto the mesh head model.

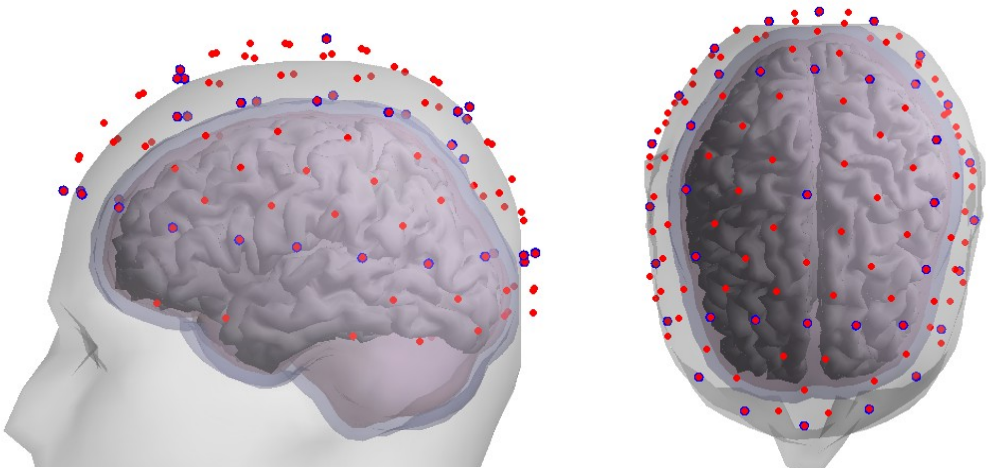

Figure 10. Three-layer head model with aligned electrodes of one subject from the side (left) and above (right).

Based on 1) the head model, 2) the source model and 3) electrode positions, signal topographies for all 16,000 sources were computed yielding a 126 x 16,000 lead field matrix L. The lead field matrix L describes how the source activity at each cortex location contributes to the electric field on the sensor array (Gordon et al., 2021).

2.5 EEG source activity estimation

Once the head model, source model and the electrode positions are available, an algorithm that is capable of projecting the EEG data from the scalp surface back to the active sources inside the brain becomes necessary.

The algorithm used in this study was the Linear Constrained Minimum Variance (LCMV) filter, which is an adapted beamforming method (Gordon et al., 2021; Van Veen et al., 1997).

Beamforming is a popular filtering method for source reconstruction of EEG data. For a source location of interest, this method computes weights for each of the numerically predefined EEG sensor locations on the scalp, which make up the spatial filter (Fig. 11). The weights are chosen in such a way that signals from other locations are attenuated while the signal from the region of interest is amplified. The final signal at the region of interest is then computed by applying the spatial filter to all the signals of the electrodes. The region of interest for the extraction of brain activity was defined as the cortical dipoles within 1 cm diameter centered in the left DMPFC (Gordon et al., 2021).

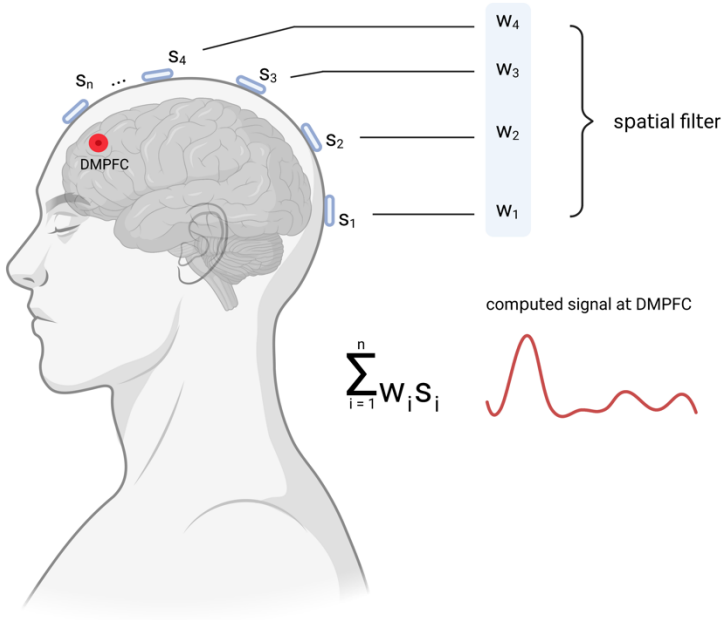

Figure 11. Illustration of a spatial filter.

For the location of interest (e.g., DMPFC), a computed weight w is assigned to each electrode of the EEG cap with the resulting vector making up the spatial filter. The signal of the region of interest is then computed by multiplication of the spatial filter and the signal s of all the scalp electrodes. Created with BioRender.com.

For the construction of this individual filter for prefrontal theta oscillations, each subject had to perform an 8 min WM task, while EEG was recorded. A signal covariance matrix C was computed from the EEG data. This procedure takes all electrodes into account, excluding the electrodes in the two outer rims, as they are often subject to interference and contribute very little to the reconstruction of the signal from the DMPFC (electrodes with labels 9 and 10 in the International 10-5 EEG system).

A covariance matrix shows how an EEG signal of one electrode position is spatially associated with the EEG signal of another electrode position (Gopan et al., 2020). It is an MxM square matrix (M being the number of channels) containing the correlation factors of the signal between each electrode pair of the EEG configuration.

For the computation of the final individual filter w, let $l(r)$ be the topography of an elementary source dipole at location r. l(r) is the r^{th} column of the lead field matrix L. Let C be the covariance matrix, then the spatial filter vector $w(r)$ to extract the activity of the source at location r is (Gordon et al., 2021; Van Veen et al., 1997):

$$w(r) = \frac{l^T(r)C^{-1}}{l^T(r)C^{-1}l(r)}$$

(1)

For the estimation of the signal in the source, let $E(t)$ be the vector of measured EEG signals at time t and $w(r)$ the spatial filter in location r , then the source amplitude $s(r,t)$ in location r at time t is obtained by:

$$s(r,t) = w(r)^{\mathrm{T}}E(t)$$

(2)

We computed the individual spatial filter w with equation (1) by only using the columns of the lead field matrix L corresponding to the dipoles in the region of interest r (left DMPFC) and used it to extract the source activity $s(t)$ in the region of interest r (left DMPFC), as described in (2) (Gordon et al., 2021).

2.6 Extraction of the SNR of prefrontal theta oscillations

EEG signals can come from either internal cortical or external sources. In order to distinguish the data from external noise (e.g., facial and eye muscle activity, power line noise) or to look at specific intrinsic frequency bands, such as theta oscillations, brain signals need to be decomposed into their separate frequency components (spectral analysis).

To extract the SNR of a frequency band, the fast Fourier transformation (FFT) is a common algorithm for the spectral analysis (Fig. 12). It decomposes an oscillatory signal into its specific frequency bands and their corresponding oscillatory power, yielding the power spectral density (PSD).

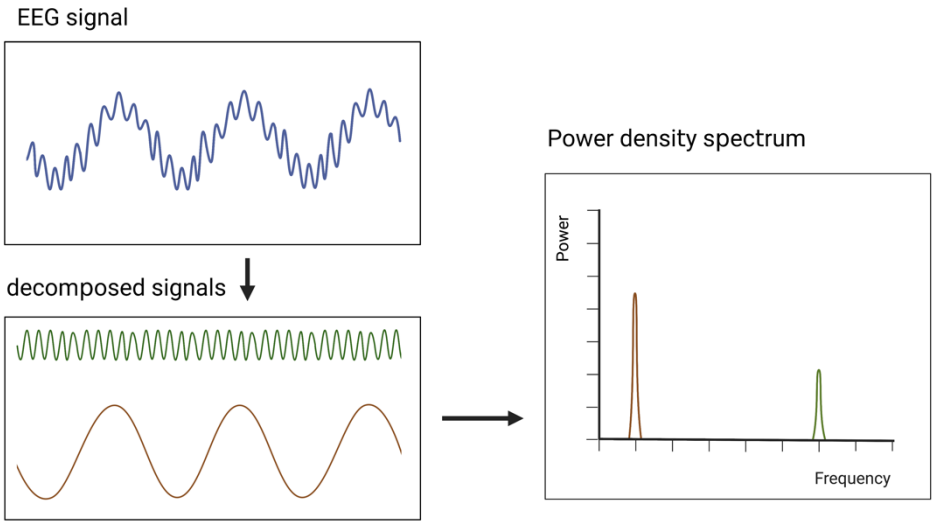

Figure 12. Illustration of the principle of Fourier Transformation.

Oscillations in EEG data are composed of different oscillations of different frequency bands. Fourier Transformation decomposes the EEG signal in its oscillatory frequency components and displays the power-frequency relation in a power density spectrum. Created with BioRender.com.

In order to increase the SNR of the theta band and consequently the sensitivity of the individualized filter w, we did not directly apply the Fourier transform to the spatially filtered data, but instead followed a multi-taper approach: The multi-taper method is used for non-time-locked oscillatory activities and tapers raw EEG data with a predefined number of tapers orthogonal to each other, so that different features of data are highlighted (Fig. 13). FFT is applied after tapering the data. The power spectra are then averaged and yield the multi-taper estimate.

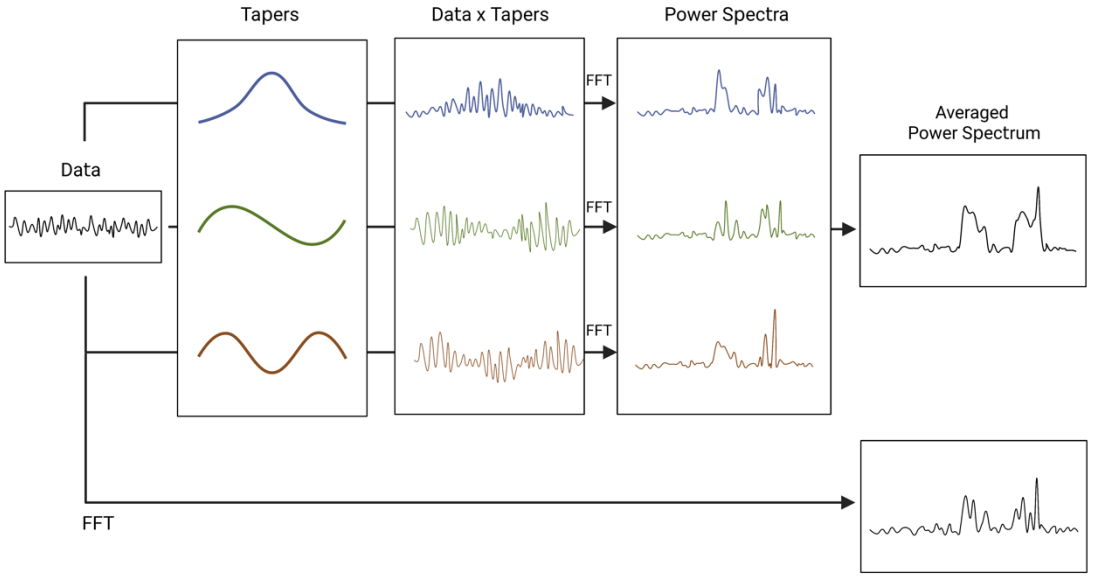

Figure 13. Illustration of the principle of multi-taper spectral analysis.

A predefined number of tapers is applied on the EEG data sequence, thus highlighting different features of the EEG signal. The power spectra of the tapered EED data are then averaged. Direct FT leads to a smoothing of EEG data, while first tapering before applying FT leads to more pronounced features of the EEG data sequence. Created with BioRender.com.

For the multi-taper analysis, 5 tapers were used on contiguous 5s data segments and a time half-bandwidth parameter of 3, which yielded a PSD of the full spectrum (Gordon et al., 2021). To further improve the SNR, aperiodic or non-oscillatory background noise was extracted from the recorded EEG data with the irregular resampling auto-spectral analysis (IRASA) method with factors 1.1-2.9 in steps of 0.1 and excluding 2.0 (Wen & Liu, 2016). The SNR was then computed by subtracting the aperiodic component from the full power spectrum (Donoghue et al., 2020). SNR was given on the log scale, in units of dB. By choosing the number of dipoles and a regularization parameter λ (how strong the filter should be applied to the data) we manually optimized the spatial filter to increase the SNR of the desired brain activity, namely prefrontal theta oscillations (Fig. 14).

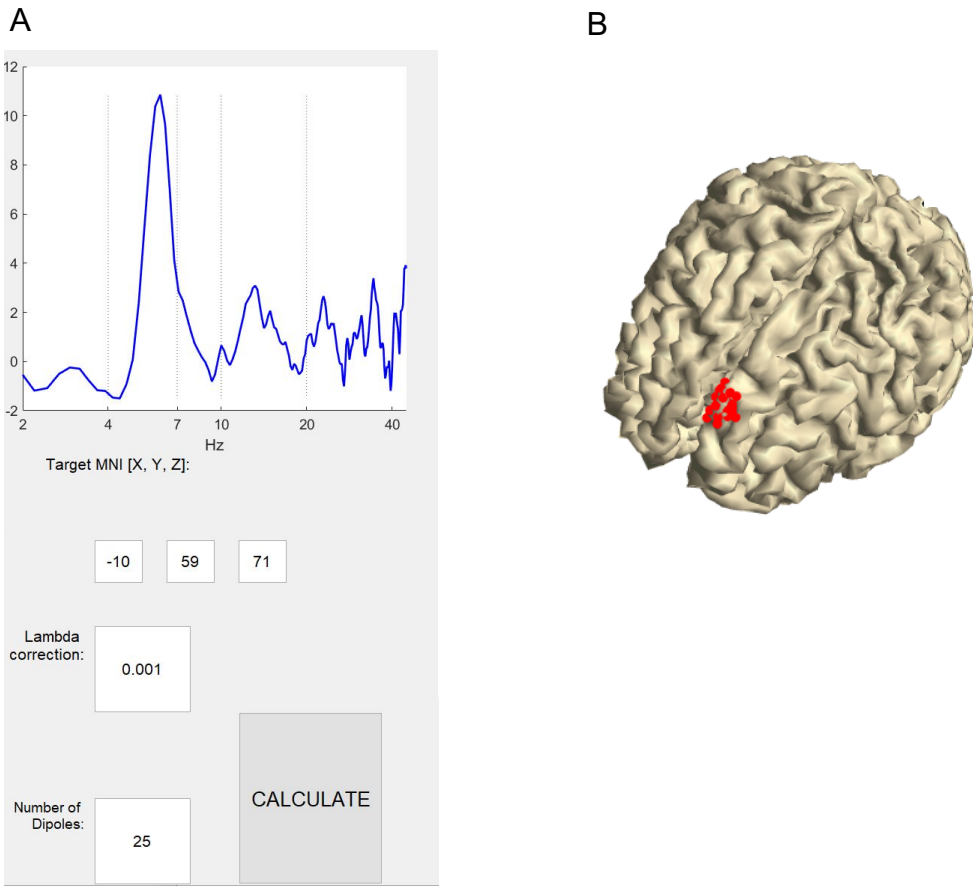

Figure 14. Computation of SNR and spatial filter w.

A: SNR [dB] of the entire power spectrum was computed for the selected dipole position. SNR of theta band for the spatial filter was optimized by setting the dipole number and a regularization parameter λ manually.

B: The positions of dipoles on the subjects MRI-reconstructed brain were selected manually for every subject with the aim to locate them in the frontal-midline area on the brain surface.

2.7 Real-time phase estimation of prefrontal theta oscillations

We obtained an estimate of the activity in the region of interest by the manually optimized spatial filter with the methods described above. We then needed to estimate the phase of the theta-oscillation in real time. To that end, we used the exact same algorithm described in the publication by Gordon et al. (2021):

The source activity signal was downsampled to 250Hz and sliding windows of data with length of 250 samples (1000ms) were analyzed by applying the following steps every 4ms to yield an instantaneous phase estimate: 1) zero-phase forward and backward filtering with an FIR (5-8Hz) band-pass filter of order

80, 2) removal of 40 samples from the epoch's window closest to the marker in order to reduce filtering edge effects, 3) autoregressive forward prediction with the Yule-Walker method (order: 20) and the total predicted interval of 500ms, 4) Hilbert transform (Gordon et al., 2021; Zrenner et al., 2020).

TMS was triggered when the estimated phase was in a predetermined range (trough: 180°±6°; random: 180°±180°) and two other conditions were met: at least 1s had passed since the previous stimulus and no signal artefacts were detected.

Those signal artefacts are defined by including four adjustable constraints: 1) eye blinks, 2) general EEG noise, 3) theta phase stability, 4) theta amplitude (Gordon et al., 2021).

1) Eye blinks were detected by computing the maximal difference of voltage potential within a 50ms sliding window between two EEG electrode pairs (Fp1-Pz, Fp2-Pz), and adding the resulting two values (one for each electrode pair). If this sum exceeded the user-defined threshold, triggering of TMS was blocked for the following 700ms (Gordon et al., 2021).
2) General EEG noise resulting from muscle artefacts, environmental noise, and movement artefacts was identified by the maximal range of signal of any of the EEG channels. If this range exceeded the user-defined threshold within a sliding window of 100ms the signal was considered too noisy (Gordon et al., 2021).
3) Theta oscillations are unstable due to phase resets and amplitude resets. Phase resets were detected by analyzing the phase progression within the sliding window of 1s with the following steps: down sampling to 250 Hz, forward and backward FIR band-pass filtering (5-8 Hz) with order 80, Hilbert transform. From the phase progression, instantaneous frequencies were determined over discrete 16ms steps. The averaged squared difference between the instantaneous frequencies across 16ms steps was computed, yielding the "oscillation stability". TMS triggers were blocked if the oscillation stability parameter went below a user-defined threshold in the previous 500ms before the trigger (Gordon et al., 2021).

4) TMS triggers were blocked if the amplitude of the ongoing theta oscillation went below the user-defined threshold, because low theta power might cause unreliable phase accuracy (Gordon et al., 2021).

The threshold for eye blinks, general EEG noise, theta phase stability and theta amplitude were set during the recording of the second part of the experiment. During the main experiment however, parameters were also adjusted manually to ensure a consistent TMS pulse application, as noise usually varied over time, mostly due to the subject's muscle contraction and blinking patterns throughout the experiment.

2.8 Real-time brain state-dependent stimulation data processing setup

A custom-built real-time system, which was executed on a xPC Target PC running the Simulink Real-Time operating system (DFI-ACP CL630-CRM mainboard) was used for real-time processing of the EEG data and triggering TMS pulses to specific phases of the ongoing oscillatory activity. The EEG data was sent to the real-time system through a real-time UDP interface at a packet rate of 5000Hz.

2.9 EEG and EMG recording

MEP in relaxed right-hand muscles were elicited by TMS applied on the hand representation of the M1 and were recorded through bipolar EMG adhesive hydrogel electrodes (Kendall, Covidien, Ireland) over the APB and FDI muscle in a bipolar belly-tendon montage (5kHz sampling rate, 0.16Hz-1.25kHz bandpass filter).

Scalp EEG was recorded with a 126-channel TMS compatible Ag/AgCl sintered ring electrode cap (EasyCap GmbH, Germany) in the International 10-20 system arrangement. The reference electrode was placed at position Cpz and the ground electrode on Afz. The skin beneath the electrodes was cleaned with an abrasive gel (Nuprep Skin Prep Gel, Weaver and Company, USA). After cleaning, the electrodes were filled with a conductive gel (Electrode Cream, Vyaire Medical Oy,

Finland). The impedances of all electrodes were kept below 10kΩ. Four 24bit 40-channel biosignal amplifiers were used for EEG and EMG recordings (NeurOne Tesla with Digital Out Option, Bittium Biosignals Ltd. Finland) at a sampling rate of 5kHz.

2.10 TMS setup

TMS was delivered with a MagPro XP Stimulator (MagVenture A/S, Denmark) connected to a figure-of-eight-coil with an inner coil winding diameter of 35mm (Cool-B65, MagVenture A/S, Denmark).

The resting motor threshold (RMT) was defined as the minimal stimulation intensity that is necessary to elicit MEPs with a 50μV peak-to-peak amplitude of the resting muscles APB and FDI in at least 5 out of 10 consecutive trials.

The neuronavigation system (Localite GmbH, Sankt Augustin, Germany) was used to locate the relative position of the coil to the subject's head in space and thus enabled stable placement of the coil on the scalp for each TMS pulse and precise targeting of the predefined cortical areas. The positions of the individual cortical target areas were predefined by MNI coordinates [left DMPFC: (-4, 52, 36) (Baetens et al., 2017; Piva et al., 2019) and right PPC: (36, -64, 38) (D'Esposito et al., 1998; Ragland et al., 2002; Wager & Smith, 2003)].

2.11 Data analysis

EEG data was analyzed with the FieldTrip open-source toolbox and customized analysis scripts on MATLAB® (Mathworks Ltd, USA, 2022a). Analyses of behavioral data and statistics were performed on MATLAB® (Mathworks Ltd, USA, 2022a).

The threshold for statistical significance was set as $p<0.05$.

2.11.1 Phase accuracy and SNR

SNR was computed as described in 2.6.

The phase accuracy was computed from the “clean” EEG data recorded in the second experimental block. The EEG matrix (channel x signal) was multiplied with the individualized spatial filter matrix and then epoched into sequences of 1000ms pre- and 1000ms post the real-time marker. For each marked trial, theta phases at the marked timepoint were extracted via Hilbert transform. Phase accuracy is reported as circular standard deviation.

2.11.2 Analysis of real-time results

Datasets of 20 subjects for session A and datasets of 14 subjects for session B were included into the analysis.

Mean response accuracies and response times for every single subject were computed for 4 conditions: 1) active TMS at theta trough, 2) sham TMS at theta trough, 3) active TMS at theta random and 4) sham TMS at theta random. Response times of subject 1 were not recorded due to technical issues. P-values were computed with the Mann-Whitney-U-test due to non-normally distributed data and were rounded to two decimal places.

2.11.3 Post-hoc analysis

In order to investigate possible effects of delivering stimuli during other phases and oscillatory patterns (theta and alpha), we used the “random phase” trials and estimated the phases at times of stimulation in a post-hoc manner. For each subject, theta phase bins were computed and summarized into 4 phase-intervals: “trough”, “peak”, “falling”, “rising” in each trial of both experimental sessions. Mean response accuracies were computed for each subject for each of those phase-intervals. Further, alpha phase bins were also computed for each subject and each trial.

In the post-hoc analysis, EEG-TMS datasets of 19 out of 20 subjects for session A could be included. The dataset of subject 15 was corrupted, hence it could not be included in the analysis. For session B, 13 out of 14 datasets were included in the post-hoc analysis. The dataset of subject 12 could not be included in the analysis due to corrupted data.

The phase estimation algorithm used in this post-hoc analysis was similar to the one from the real-time estimation. The EEG data was multiplied with a spatial filter of interest and then epoched into sequences of 1000ms to 10ms pre-stimulus to exclude the TMS artefact. After the data was down sampled to 250Hz, a FIR band-pass filter of order 80 (alpha 8-12Hz or theta 5-8Hz) was applied. 40 samples from the epoch's window closest to the marker were removed, followed by an autoregressive forward prediction of order 20 (Yule Walker method), and then followed by the Hilbert transform.

The EEG data was spatially filtered in two ways to obtain the phase of the theta oscillation: with 1) individualized spatial filter w and with 2) channel Afz (Berger et al., 2019). The signal which the alpha phase was extracted from was obtained with a Laplacian filter from the channel cluster CP6, CP4, TP8, P6 and C6, representing the right PPC area of the cortex. P-values were computed with the Kruskal-Wallis-test and were rounded to two decimal places.

3 Results

3.1 Phase accuracy and SNR

We tested the accuracy of the phase detection method. This is of considerable importance, as it informs on how consistently the TMS pulses were delivered during the desired phase of the theta oscillation. The average phase accuracy of the TMS application, which targeted the trough of theta in the experiments, across all subjects had a mean of 190° and a standard deviation of 59° (Fig. 15). Around 40% of the pulses were delivered at the theta trough 180° ± 30°.

As described by a previous study by Zrenner et al., 2020, one of the major predictors of the phase detection method's accuracy is the SNR of the targeted oscillation. In our study, the SNR of the theta band varied largely among subjects, but remained robust within experimental sessions of single subjects (Fig. 16). The mean SNR across all subjects was 5.4dB. As predicted, the theta SNR of a subject was a strong indicator of the phase-detection method's accuracy. Figure 17A demonstrates the phase accuracy of 2 subjects with different theta SNR.

Higher theta SNR correlated with lower standard deviation, thus making the phase detection and triggering of the real-time algorithm more precise (Fig. 17B).

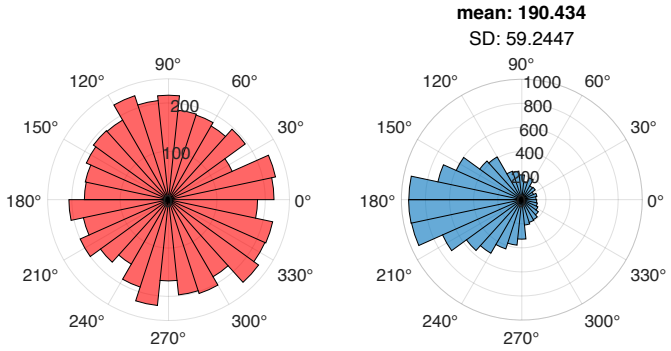

Figure 15. Response accuracy of all random (red) and trough (blue) trials

Polar histograms showing the sum of all phase bins of all random trials (red) and trough trials (blue) across all subjects and sessions. Trough is defined as 180°. Radius of the polar histogram shows the number of stimulated trials.

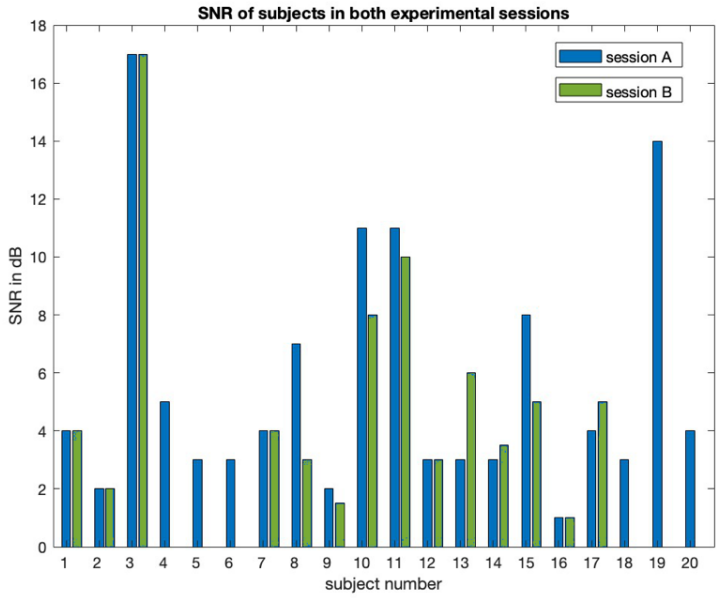

Figure 16. SNR distribution of all subjects in both experimental sessions A (blue) and B (green).

X-axis shows the subject number of all subjects in both experimental sessions. Y-axis shows the corresponding theta band SNR [dB].

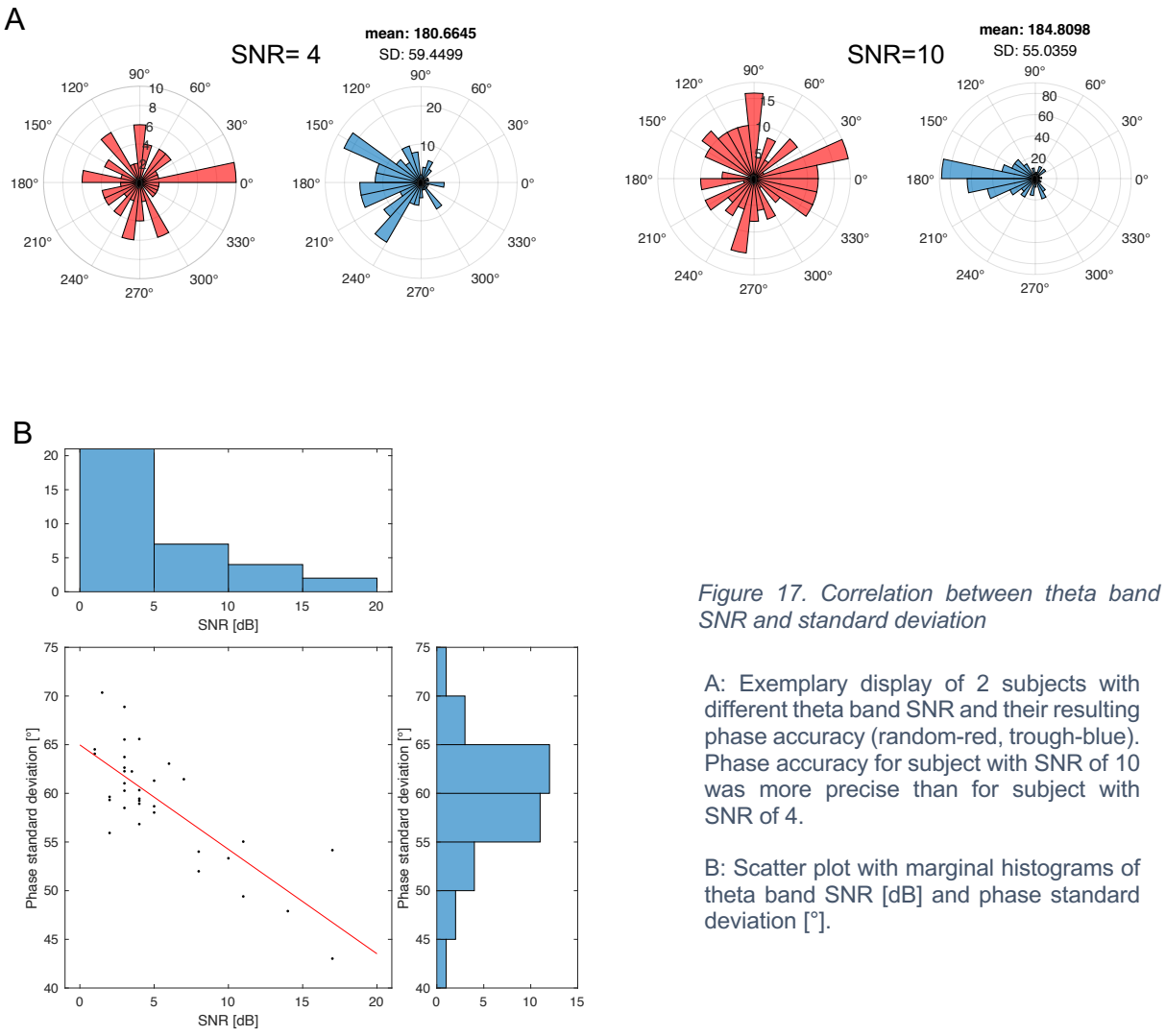

Figure 17. Correlation between theta band SNR and standard deviation

A: Exemplary display of 2 subjects with different theta band SNR and their resulting phase accuracy (random-red, trough-blue). Phase accuracy for subject with SNR of 10 was more precise than for subject with SNR of 4.

B: Scatter plot with marginal histograms of theta band SNR [dB] and phase standard deviation [°].

3.2 Real-time response accuracy and time of session A (Stimulation of PPC)

3.2.1 Sternberg WM task

We proceeded to apply TMS to the PPC, which involved both “sham” and “active” TMS conditions, each containing pulses applied during either the trough of the theta band or at random time points. According to our hypothesis, for the active conditions we expected a decline of the response accuracy and an increase of the response time when active TMS is applied to the trough of prefrontal theta in

comparison to random phase stimulation. Moreover, for the sham conditions, we expected response accuracy and response time to be similar between the theta trough and random phase conditions.

We observed that delivering active TMS applied to the PPC, irrespective of whether the pulses occurred during the trough of the ongoing prefrontal theta oscillation or at random phase, had no significant impact in response accuracy or response time of the Sternberg WM task (Mann-Whitney/rank-sum, $p>0.05$, $df=19$). Likewise, there was no significant effect when the applied stimulus was provided by the sham TMS ($p>0.05$) (Fig. 18).

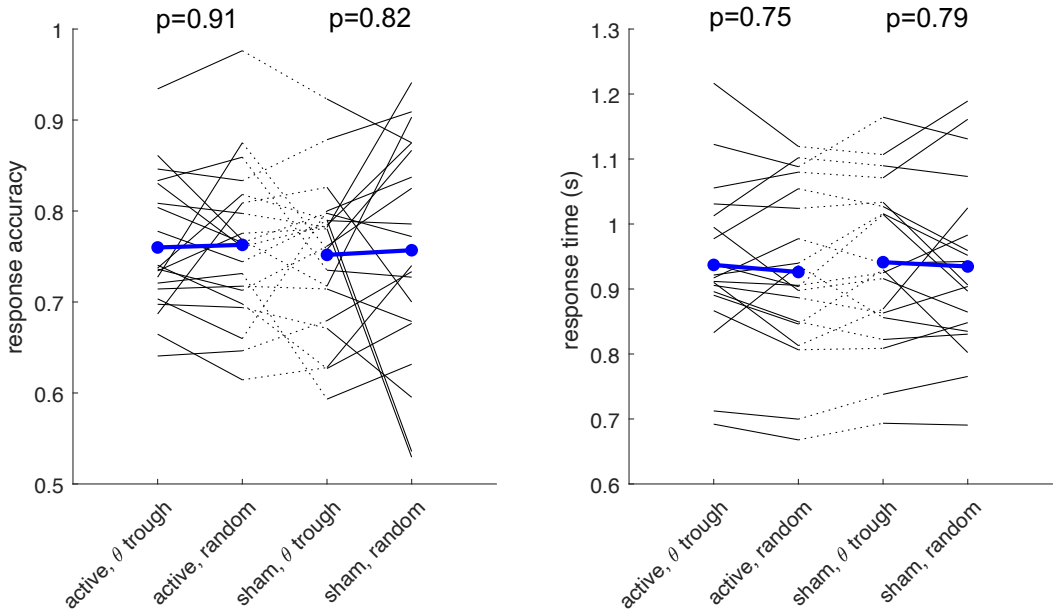

Figure 18. Response accuracy and response time with regard to the experimental conditions of the Sternberg WM task in session A.

Left: Y-axis shows response accuracy. Right: Y-axis shows response time [s]. X-axis shows all four experimental conditions. Black lines display the mean response accuracy and mean response time of one subject for the trough and random phase condition. Blue dots and lines represent the mean response accuracy and response time among all subjects. Mann-Whitney-U-test does not yield significant results of response accuracy and time with regard to the phase for both active and sham conditions.

3.2.2 Visuospatial WM task

Similar to the Sternberg WM task, we expected a decline of response accuracy and an increase of response time after active TMS applied to the trough of prefrontal theta in comparison to the random phase condition. We also expected

response accuracy and response time to be similar between the trough and random phase condition for the sham conditions.

Moreover, we expected a stronger phase related effect of active TMS on WM for the “mirrored” visuospatial task type, as this task required mental manipulation of information, and thus more frontal executive processing compared to the “identical” task type.

3.2.2.1 Identical

We observed that delivering active TMS applied to the PPC, irrespective of whether the pulses occurred during the trough of the ongoing prefrontal theta oscillation or at random phase, had no significant impact in response accuracy or response time of the identical visuospatial WM task (Mann-Whitney/rank-sum, $p>0.05$, $df=19$). Likewise, there was no significant effect when the applied stimulus was provided by the sham TMS ($p>0.05$) (Fig. 19).

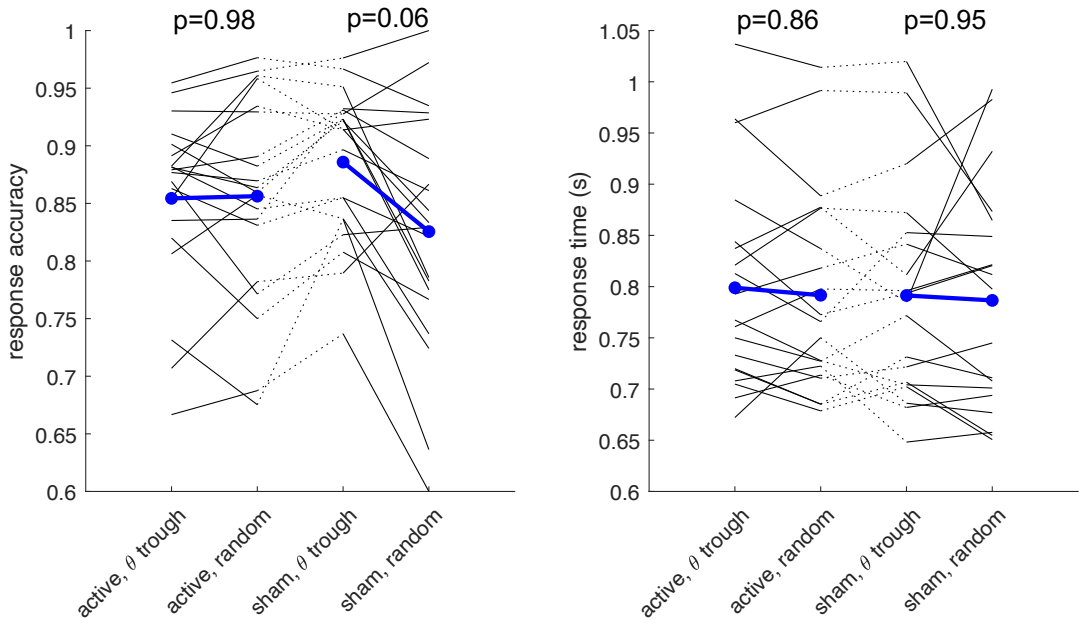

Figure 19. Response accuracy and response time with regard to the experimental conditions of the identical visuospatial WM task in session A.

Left: Y-axis shows response accuracy. Right: Y-axis shows response time [s]. X-axis shows all four experimental conditions. Black lines display the mean response accuracy and mean response time of one subject for the trough and random phase condition. Blue dots and lines represent the mean response accuracy and response time among all subjects. Mann-Whitney-U-test does not yield significant results of response accuracy and time with regard to the phase for both active and sham conditions.

3.2.2.2 Mirrored

We observed that delivering active TMS applied to the PPC, irrespective of whether the pulses occurred during the trough of the ongoing prefrontal theta oscillation or at random phase, had no significant impact in response accuracy or response time of the mirrored visuospatial WM task (Mann-Whitney/rank-sum, $p>0.05$, $df=19$). Likewise, there was no significant effect when the applied stimulus was provided by the sham TMS ($p>0.05$) (Fig. 20).

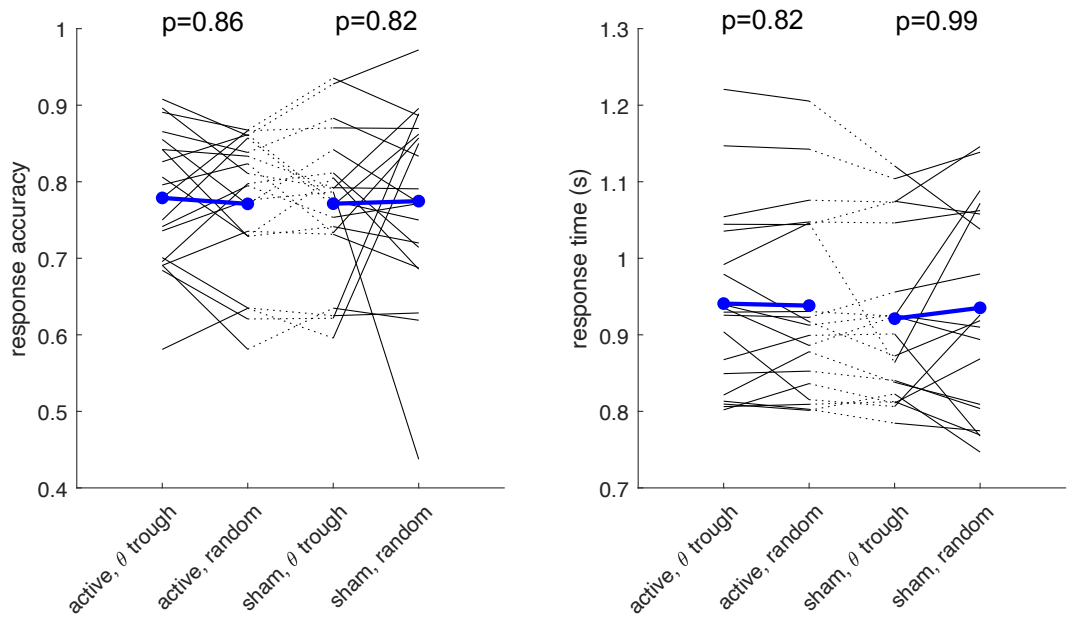

Figure 20. Response accuracy and response time with regard to the experimental conditions of the mirrored visuospatial WM task in session A.

Left: Y-axis shows response accuracy. Right: Y-axis shows response time [s]. X-axis shows all four experimental conditions. Black lines display the mean response accuracy and mean response time of one subject for the trough and random phase condition. Blue dots and lines represent the mean response accuracy and response time among all subjects. Mann-Whitney-U-test does not yield significant results of response accuracy and time with regard to the phase for both active and sham conditions.

3.3 Real-time response accuracy and time of session B (Stimulation of DMPFC)

3.3.1 Sternberg WM task

We proceeded to repeat the procedures described for the PPC stimulation, but now targeting the DMPFC as another cortical area of the FPN executing top-down control on the PPC. For the active conditions in this session, we thus

expected an improvement of response accuracy and a decrease of response time after active TMS applied to the trough of prefrontal theta in comparison to the random phase condition. We expected response accuracy and response time to be similar between the trough and random condition for the sham conditions.

We observed that delivering active TMS applied to the DMPFC, irrespective of whether the pulses occurred during the trough of the ongoing prefrontal theta oscillation or at random phase, had no significant impact in response accuracy or response time of the Sternberg WM task (Mann-Whitney/rank-sum, $p>0.05$, $df=13$). Likewise, there was no significant effect when the applied stimulus was provided by the sham TMS ($p>0.05$) (Fig. 21).

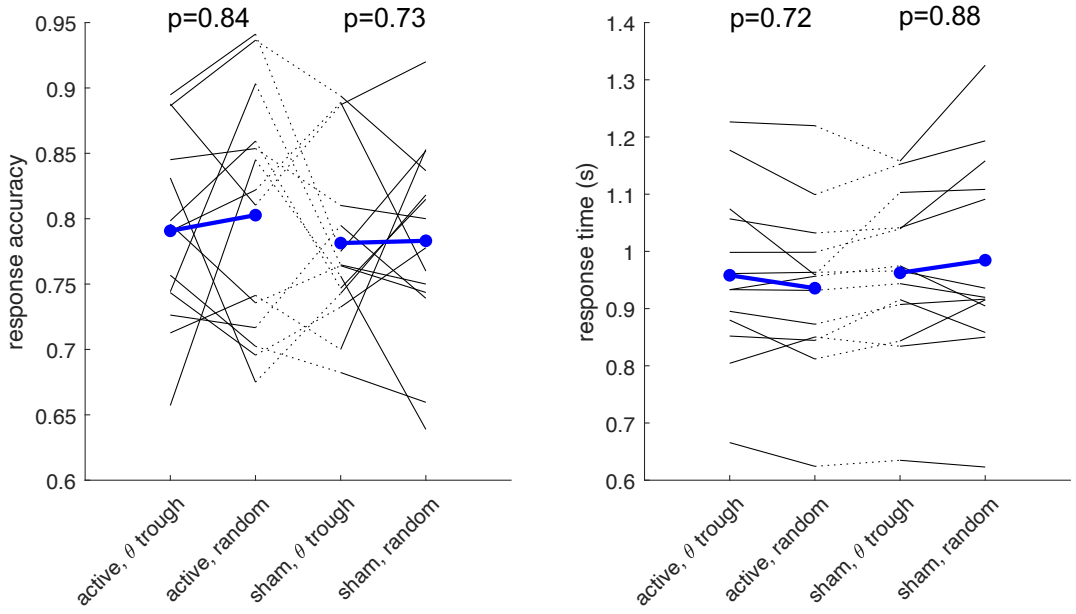

Figure 21. Response accuracy and response time with regard to the experimental conditions of the Sternberg WM task in session B.

Left: Y-axis shows response accuracy. Right: Y-axis shows response time [s]. X-axis shows all four experimental conditions. Black lines display the mean response accuracy and mean response time of one subject for the trough and random phase condition. Blue dots and lines represent the mean response accuracy and response time among all subjects. Mann-Whitney-U-test does not yield significant results of response accuracy and time with regard to the phase for both active and sham conditions.

3.3.2 Visuospatial WM task

Similar to the Sternberg WM task, we expected an improvement of response accuracy and a decrease of response time after active TMS applied to the trough

of prefrontal theta in comparison to the random phase condition. We expected response accuracy and response time to be similar between the trough and random phase condition for the sham stimulation.

We expected a stronger phase related effect of active TMS on WM for the mirrored compared to the identical visuospatial task type.

3.3.2.1 Identical

We observed that delivering active TMS applied to the DMPFC, irrespective of whether the pulses occurred during the trough of the ongoing prefrontal theta oscillation or at random phase, had no significant impact in response accuracy or response time of the identical visuospatial WM task (Mann-Whitney/rank-sum, $p>0.05$, $df=13$). Likewise, there was no significant effect when the applied stimulus was provided by the sham TMS ($p>0.05$) (Fig. 22).

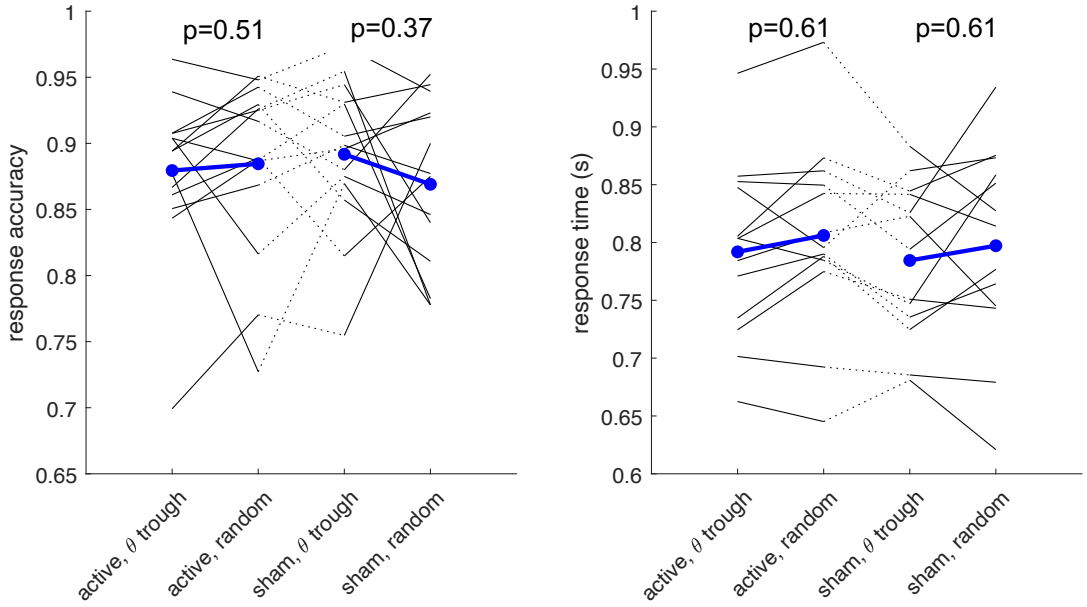

Figure 22. Response accuracy and response time with regard to the experimental conditions of the identical visuospatial WM task in session B.

Left: Y-axis shows response accuracy. Right: Y-axis shows response time [s]. X-axis shows all four experimental conditions. Black lines display the mean response accuracy and mean response time of one subject for the trough and random phase condition. Blue dots and lines represent the mean response accuracy and response time among all subjects. Mann-Whitney-U-test does not yield significant results of response accuracy and time with regard to the phase for both active and sham conditions.

3.3.2.2 Mirrored

We observed that delivering active TMS applied to the DMPFC, irrespective of whether the pulses occurred during the trough of the ongoing prefrontal theta oscillation or at random phase, had no significant impact in response accuracy or response time of the mirrored visuospatial WM task (Mann-Whitney/rank-sum, $p>0.05$, $df=13$). Likewise, there was no significant effect when the applied stimulus was provided by the sham TMS ($p>0.05$) (Fig. 23).

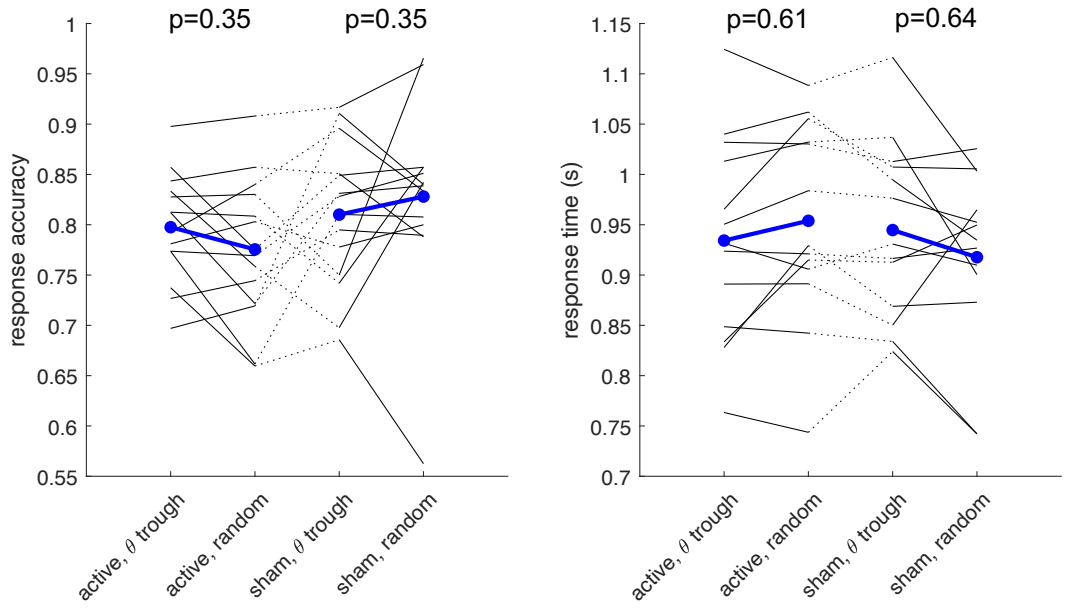

Figure 23. Response accuracy and response time with regard to the experimental conditions of the mirrored visuospatial WM task in session B.

Left: Y-axis shows response accuracy. Right: Y-axis shows response time [s]. X-axis shows all four experimental conditions. Black lines display the mean response accuracy and mean response time of one subject for the trough and random phase condition. Blue dots represent the mean response accuracy and response time among all subjects. Mann-Whitney-U-test does not yield significant results of response accuracy and time with regard to the phase for both active and sham conditions.

3.4 Post-hoc phase analysis

We finally proceeded to compare the behavioral results of TMS to the PPC and DMPFC during different phases of the theta oscillation cycle, namely the through, the peak, the rising and the falling phases. This was done by taking both the "active" and "random" stimulation condition and performing a post-hoc estimation of the theta phase during which each pulse was delivered. The signal used for

this analysis was yielded by the individual w-filter. In order to confirm the results, we also repeated the analyses using the signal from a single electrode placed over the DMPFC, namely the Afz channel.

The post-hoc analysis did not yield significant differences (Kruskal-Wallis/rank-sum, $p>0.05$) between the four chosen phase-intervals (peak, rising, trough, falling) of prefrontal theta oscillations, neither extracted from the spatial filter w nor extracted from the channel Afz and the response accuracy in the Sternberg and visuospatial WM tasks for both sessions A and B (Fig. 24, 25).

Lastly, we tested for the possibility of the behavioral performances being more sensitive to phase-dependent effects of TMS of another oscillatory activity. Specifically, posterior-parietal alpha oscillations are believed to play an important role in WM maintenance. Therefore, we repeated the analyses with post-hoc phase estimation of the alpha oscillation from the left PPC, extracted with a Laplacian filter from the electrodes CP6, CP4, TP8, P6 and C6. For the alpha-band phase, no significant differences (Kruskal-Wallis/rank-sum, $p>0.05$) of the four phase-intervals could be found in regard to response accuracy of both WM task types for both sessions A and B (Fig. 24, 25).

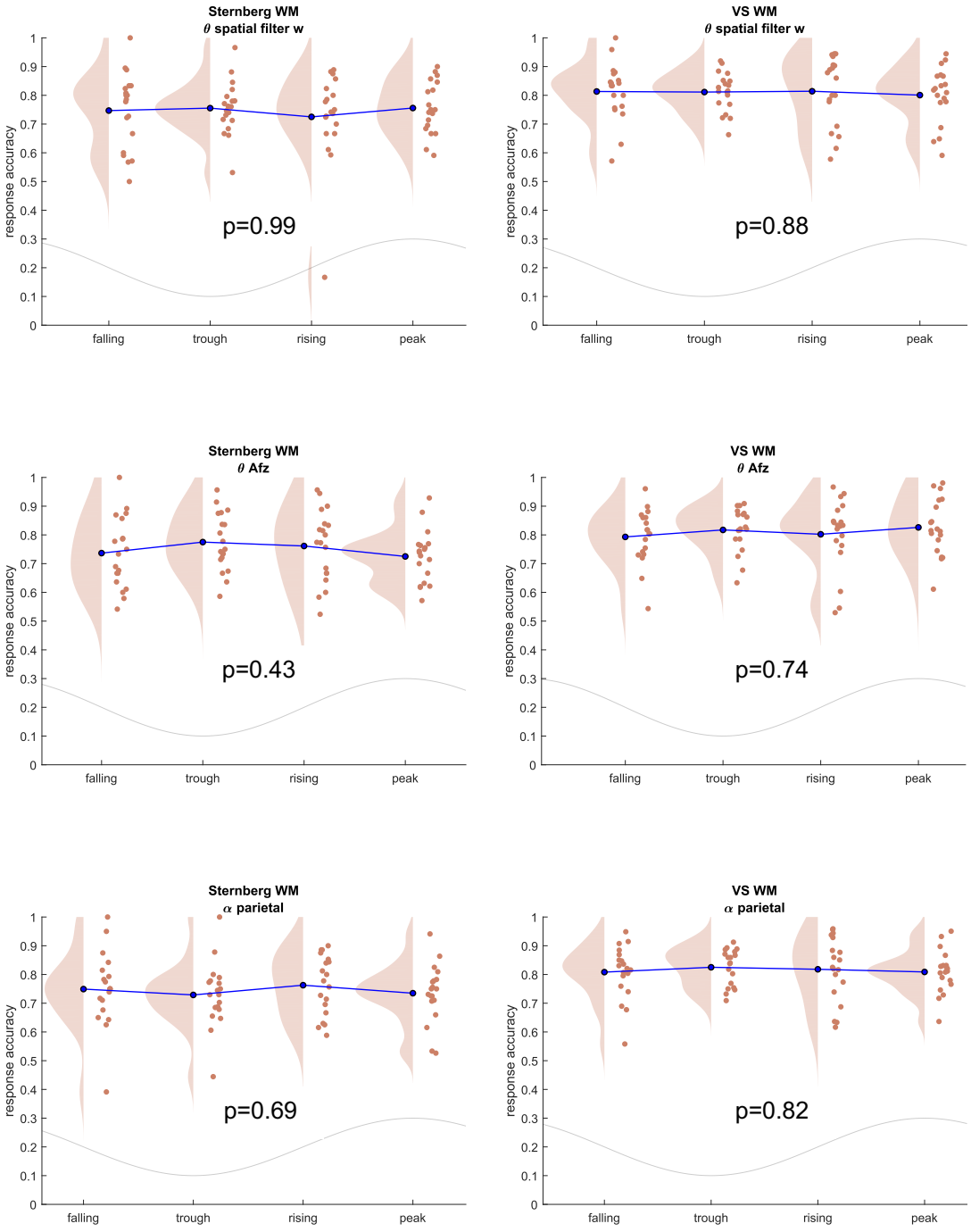

Figure 24. Response accuracy with regard to post-hoc estimated phases in session A.

Display of the mean response accuracy for every subject for the Sternberg and visuospatial WM tasks with regard to the post-hoc estimated phase of theta (Afz), theta (filter w) and alpha (posterior-parietal) oscillation.

Y-axis shows response accuracy. X-axis shows all 4 phase-intervals: 1-falling, 2-trough, 3-rising, 4-peak. Red dots represent the mean response accuracy of individual subjects. Blue dots show the mean of response accuracy of all subjects. Kruskal-Wallis-test does not yield significant differences for response accuracies for the four phase-intervals.

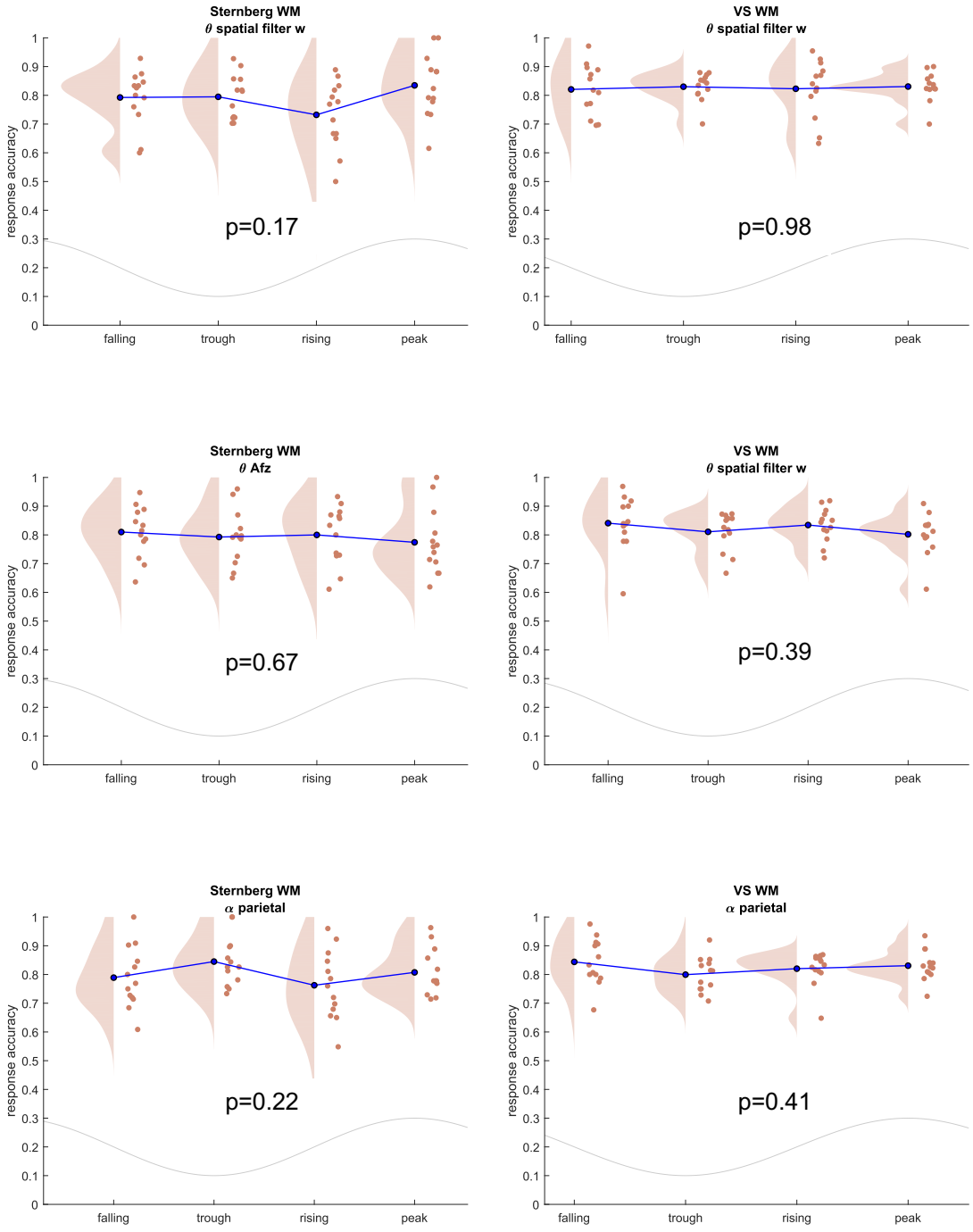

Figure 25. Response accuracy with regard to post-hoc estimated phases in session B.

Display of the mean response accuracy for every subject for the Sternberg and visuospatial WM tasks with regard to the post-hoc estimated phase of theta (Afz), theta (filter w) and alpha (posterior-parietal) oscillation.

Y-axis shows response accuracy. X-axis shows all 4 phase-intervals: 1-falling, 2-trough, 3-rising, 4-peak. Red dots represent the mean response accuracy of individual subjects. Blue dots show the mean of response accuracy of all subjects. Kruskal-Wallis-test does not yield significant differences for response accuracies among subjects for the four phase-intervals.

3.5 Post-hoc analysis of sensory effects on behavioral outcome

It is worth mentioning that a few subjects dropped out of session B because of the unpleasant sensation by TMS and the electrical stimulation at the stimulated area (stimulation at the PFC was generally perceived as more painful than stimulation at the PPC). Sensory inputs can be distractors while performing cognitive tasks. Hakim et al. (2021) for example reported that visual distractors presented in the retention period of a visual WM task led to WM impairment of subjects. We therefore computed phase accuracies and response times for all stimulated trials (regardless of TMS and electrical stimulation) and all non-stimulated trials in both experimental sessions for all subjects (Fig. 26). Since the stimulation in session B was in general reported to be more intense and more painful than the stimulation in session A, we expected stronger effects in session B. Indeed, we found a trend towards significant impact (Mann-Whitney/rank-sum, p=0.05) of stimulation on the response time for subjects performing the visuospatial task in session B. Interestingly, subjects seemed to perform faster in stimulated trials with no notable increase of response accuracy. For the Sternberg task in session B though, the effect was non-significant. Since subjects had to memorize and respond faster in the visuospatial tasks than in the Sternberg tasks due to shorter time frames, one could argue that this condition was more sensitive to external effects.

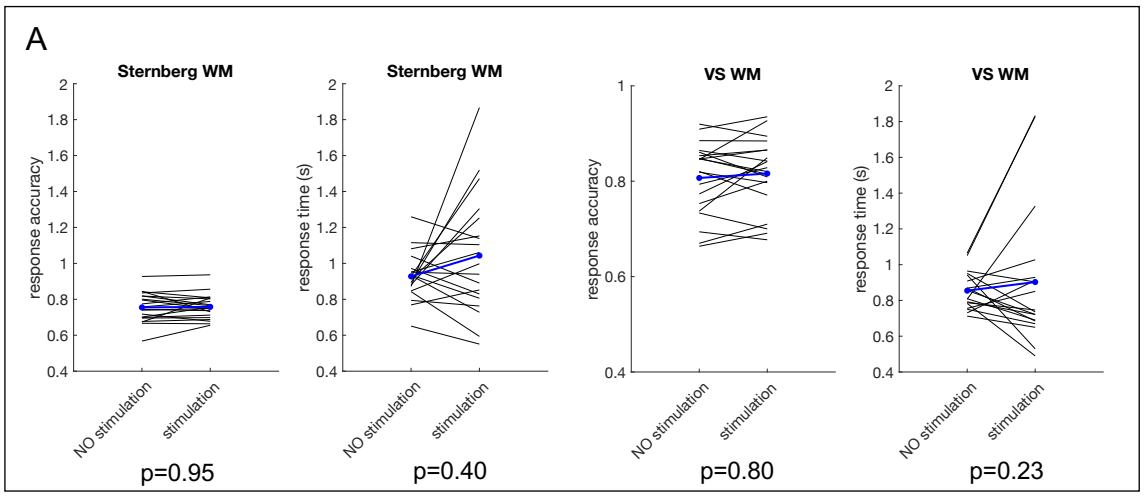

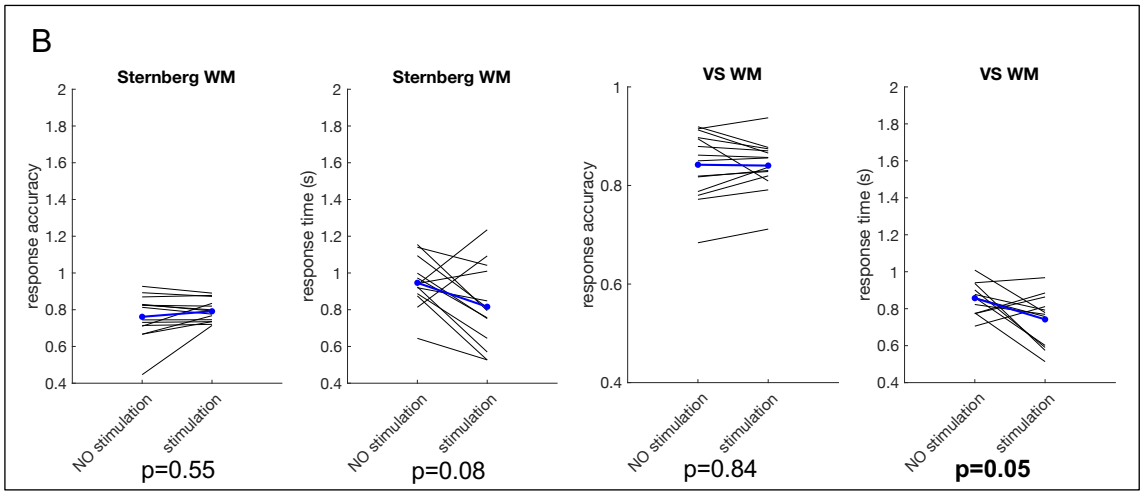

Figure 26. Response accuracy and response time for all stimulated trials (both TMS and electrical stimulation) and non-stimulated trials for all subjects in both sessions A (PPC stimulation) and B (DMPFC stimulation).

Y-axis shows the response accuracy. X-axis shows two conditions, either all stimulated trials or all non-stimulated trials. In session A, response accuracy and response time remained robust with and without stimulation. In session B, subjects responded faster in stimulated trials than in non-stimulated trials, only in visuospatial tasks. A similar trend can be observed in the Sternberg task. P-values were computed with the Mann-Whitney-U-test.

3.6 Post-hoc analysis of time delays of delivered TMS pulses

The marker for triggering the TMS triple pulse was set 700ms after the memory set offset within the retention period. If the detected prefrontal theta oscillation showed a sufficient amplitude and phase stability, and overall EEG signal contained low interference, a TMS pulse was delivered. If the conditions were not met, the pulse delivery was delayed. The time delay of applied pulses in all experimental trials is presented in Fig 27. Most pulses (>50%) were delivered within the first 1800ms after memory set offset in the Sternberg task and 1200ms in the visuospatial task.

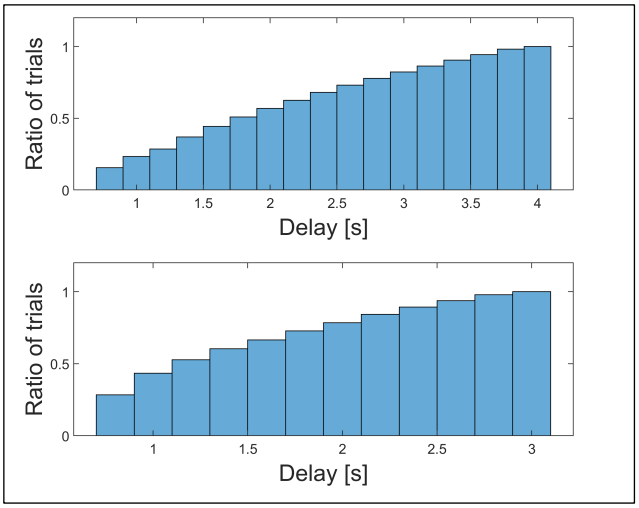

Figure 27. Time delay of delivered TMS pulses of all trials in the Sternberg task (above) and the visuospatial task (below).

Y-axis shows the cumulative ratio of trials. *X*-axis shows the time delay [s] of the delivered pulses.

4 Discussion

The objective of this study was to influence the behavioral output during a cognitive task performance by delivering brain stimulation at specific cortical regions and time points. Specifically, it meant targeting the trough of ongoing prefrontal theta oscillations during a WM task to modulate behavioral outcomes on WM performance.

The trough phase of neuronal oscillations in the theta band has been hypothesized to represent a state of high neuronal excitability. Theta band oscillations show an increased activity during cognitive tasks. Cortical regions associated with the FPN (right PPC, left DMPFC) show increased functional connectivity in the theta band during cognitive task performances. By stimulating the right PPC and the left DMPFC with TMS at the trough phase of prefrontal theta we attempted to modulate neuronal communication within the FPN.

Previously, Berger et al., (2019) carried out a similar experiment, but using random TMS pulses and post-hoc offline phase estimation. They observed a decrease in WM phase accuracy when TMS occurred in the theta trough during the retention period. In our study we attempted to go one step further by implementing that concept in an online brain state-dependent stimulation design, which meant being able to control behavioral output in real-time.

Given the meaningfulness of properly delivering stimuli in specific phases of ongoing cortical oscillations as explained by the communication through coherence theory (Fries, 2015), the present study involved methods that allowed precise stimulation during specific theta phases originating from the prefrontal cortex. This was achieved by creating an individualized spatial filter w for each subject based on their anatomy and their brain activity, aiming to maximize the SNR of the prefrontal theta band.

In our study, we did not observe a significant impact on WM performance by the real-time delivery of TMS triple pulses during the trough of the prefrontal theta-rhythm at either the right PPC nor the left DMPFC. This goes against our hypotheses and the results observed by Berger et al., (2019). Possible reasons for these negative results will be discussed below.

One possibility is that the variability in the phase accuracy for stimulation was inappropriate for the present purposes. However, it is unlikely that the phase accuracy accounts for these negative results, as the overall phase accuracy of the real-time TMS application in this study was comparable to a previous brain state-dependent EEG-TMS study targeting prefrontal theta with the same paradigm at resting state, suggesting that it is possible to observe electrophysiological and behavioral effects from applying TMS pulses to different phases of ongoing cortical oscillations at these phase accuracy ranges (Gordon et al., 2022; Gordon et al., 2021; Zrenner et al., 2018).

Nevertheless, single subjects with a low SNR might have received TMS stimulation at an improper time point more frequently, leading to no effect on their behavioral outcome. There is a high variability of results on the subject level as a lower SNR resulted in less accurate phase detection and TMS triggering as already shown in other studies (Gordon et al., 2021; Zrenner et al., 2020). This is plausible, as a weak SNR implies a less pronounced signal compared to other noisy signals, thus being less precisely detectable by the real-time algorithm. Since we did not include a prior subject selection according to the SNR, the theta band SNR and the correlating phase accuracy in experimental sessions varied greatly among subjects. On the other hand, the average SNR among subjects

was comparable to the study by Gordon et al., (2021). Further, even after the post-hoc extraction of the theta phases of all active trials and reassigning the trials to the corresponding behavioral results, results still remained negative.

Moreover, it is also possible that the number of stimulated trials was not sufficient. As the number of stimulated trials correlated with the size of the theta band SNR and the resulting phase accuracy, it varied greatly among subjects. The real-time algorithm only allowed TMS triggering if the phase of the signal input could be detected and if all constraints (eye blinks, general EEG noise, theta phase stability and theta amplitude) were fulfilled. A pronounced and more stable theta signal naturally could be detected easier among other noisy signals. This meant that higher SNR in the experiment led to more trials with active stimulation. Experiments with subjects of very low SNR therefore included a low number of triggered trials, thus lacking in statistical power. Therefore, we analyzed the results of only the subjects with high SNR, but the results were still negative.

It should also be noted that, as the experiment proceeded over time, the signal quality of the electrodes declined, which is most likely due to the drying of the electrodes gel and consequent increase in impedance (Liu et al., 2019). Subjects also became increasingly tired and muscle activity increased, which also compromised the signal quality. Despite breaks and impedance quality check-ups of the electrodes, a steady decline of signal quality could not be prevented. The declining signal quality led to more imprecise triggering and fewer triggered trials, thus imposing a limit to the total number of stimulated trials per session. However, in the analysis the number of stimulated trials was adequate among subjects in the experiment. Additionally, in order to increase statistical power, the post-hoc analysis was also performed to include trials of the random condition, in which the trough was randomly targeted, into the theta trough analysis. Still, the post-hoc analysis yielded negative results.

In summary, it is unlikely that these technical issues can explain the negative results.

Apart from technical issues, other aspects might explain the negative findings. The present focus on the trough phase stimulation might have led us to neglect

the importance of other oscillatory phases, which if interfered with could then lead to real-time behavioral changes. However, post-hoc results show that tested WM performances were not affected by stimulation during any specific phase (falling, trough, rising, peak) of the prefrontal theta rhythm. Moreover, this was not supported by the findings from Berger et al., (2019), who observed an impairment of varying size on visuospatial working memory by TMS, depending on the phase of stimulation. In their study, it has been shown post-hoc that the impairment of the visuospatial WM performance is the strongest if TMS is applied to the right hemispheric PPC at the trough of the prefrontal theta rhythm. For their theta phase analysis, Berger et al., (2019) used the signal of the channel Afz, thus differing from our approach with the individualized spatial filter w. So as another attempt, we also extracted the theta phases of our study post-hoc from the Afz channel, but our results still were negative.

Moreover, since Berger et al., (2019) only used a single channel Afz for theta signal extraction instead of an individualized spatial filter, it could be possible that they measured volume-conducted alpha from posterior regions instead of theta oscillations, given the often considerably higher SNR of posterior alpha. Previous studies have also provided evidence that it is not only the frontoparietal coherence of the theta band but also the alpha band that plays an important role in attention focusing and memory processing (Klimesch et al., 2011; Klimesch et al., 1994; Roux & Uhlhaas, 2014; Sauseng et al., 2005). Both frequencies are proposed to encode different information classes. This is the reason, why we also analyzed the phase of posterior alpha oscillations of the right PPC in a post-hoc manner, but the results did not reveal any significant information about the impact of the alpha band on WM.

To better explain why we could not impact WM function with this study paradigm, it is important to revisit the scientific status quo about the mechanisms of WM in other EEG-TMS and behavioral studies.

Berger et al., (2019) proposed that frontoparietal interaction relevant for WM particularly takes place within short periodic time windows. Those time windows are proposed to be determined by the FM-theta and temporo-parietal gamma

synchronization, which modulate the strength of communication between frontal and parietal regions. According to this theory, if a TMS pulse is delivered at a phase of high excitability, namely theta trough, the coupling of FPN network is disturbed and thus the maintenance of WM item representations is impaired. Further, the oscillations of FM-theta clock a gating mechanism for enabling the DMPFC to access the PPC and vice versa, a prerequisite for maintaining WM items in memory and thus WM function (Berger et al., 2019).

This phase-related effect however could have been masked or disrupted by the strong sensory distraction by the TMS pulses and electrical stimulation in our experiment, as shown in the post-hoc analysis of sensory effects on behavioral outcome. Indeed, we found that short-term and strong sensations by stimulation of any type might have increased alertness and focus for a while, thereby explaining the improved reaction time, but not improved WM retention for the visuospatial task. These results indicate that alertness (pressing the response box button as soon as possible after the signal) and WM processing (memorizing WM items and maintaining them correctly) can be affected independently from each other. Further, they highlight the relevance of alertness for the execution of WM tasks.

Besides WM processing, FM-theta is also associated with alertness or attention. For instance, Duprez et al. (2020) suggested that FM-theta oscillations clock a variety of cortical processing mechanisms, including attention modulation and inhibitory control. Similar to the oscillation-based gating mechanism of WM in the FPN, an oscillation-based mechanism has been observed for visual perception. The visual perception system seems to involve time windows in which perception is periodically enhanced (VanRullen, 2016). This sampling of perception is proposed to underlie the periodic allocation of attention that directs attention to visual information, thus enhancing the perception periodically. This cycle is aligned with the rhythm of slow brain oscillations, such as FM-theta (Busch & VanRullen, 2010). Hence, FM-theta oscillations and attention are strongly linked with each other, as shown in many studies (Benchenane et al., 2011; Fiebelkorn & Kastner, 2019; Fiebelkorn et al., 2018; Gregoriou et al., 2009).

Further, there is a time window called the attentional blink, which is frequently referred to an impairment in post-perceptional processing (Luck et al., 1996). The attentional blink is a 200 millisecond time window 400-600ms after the detection of a target stimulus in a rapid stream of visual stimuli, in which further newly presented stimuli are less likely registered by subjects and are thus missed. Hence, attentional processes underlying the selection of perceptual information are different from attentional processes responsible for the selection of more highly processed conceptual information, as perceptual and post-perceptual processing occur in different time windows after the presentation of a stimulus (Luck et al., 1996).

So, it might be that WM processing could only be sensitive to theta oscillation-related effects in the first hundreds of milliseconds in the retention period before the attentional blink. This means that TMS pulses might have been delivered in an insensitive time window of the retention period and thus could not affect relevant attentional processes. In our experiment, triple pulses were delivered 700ms after memory set offset within the retention period time window. Also, since the timing of the triggered TMS pulses by the real-time algorithm varied greatly due to delay by noisy signals for example, TMS might have led to an inconsistent effect on WM performance. Nevertheless, the latency and variability are also consistent with the experiment of Berger et al., (2019), as the onset of triple pulses was jittered between 500-1500ms after memory set offset and, therefore, do not explain the discrepancy in the results between the two studies.

Here, the inevitable question arises of how attention and WM actually relate to each other. There are several cognitive models of WM that describe the interaction between memory and attention. A common idea of these models is that the items of WM are internal representations from long-term memory (LTM) that are contemporarily activated by the focus of attention (Cowan, 1995; D'Esposito & Postle, 2015). During the encoding period, internal representation of items of LTM are accessed through perceptional recognition. During the retention period, those representations are then maintained in an elevated state of activation by the focus of attention until the information is no longer available (Cowan, 1995; D'Esposito & Postle, 2015). Thus, the focus of attention on internal

representations (semantic, sensory, motoric) reflects a necessary process which enables the short-term retention in WM (D'Esposito & Postle, 2015).

It also could be the case that phase-related effects can only be observed in even earlier stages, such as the encoding period, during which the oscillatory activity guides attention and encoding of stimuli, whereas in the retention period the information might be embedded differently:

It has been proposed that persistent neuronal activity in the PFC serves as a requirement for WM (D'Esposito & Postle, 2015). Instead of serving as the gatekeeper for allowing access to internal representations, theta oscillations in the retention period are also thought to encode WM content (Axmacher et al., 2010). Thus, a disrupted chain of the oscillatory activity in the retention period caused by TMS then would consequently result in a loss of WM content. Recently however, some studies have suggested the contrary: that persistent neuronal activity in the delay period in the prefrontal region might not be necessary for WM maintenance (Lorenc et al., 2021; Stokes, 2015). Indeed, it has been shown that not all WM content is reflected in the neuronal oscillations, even when it is still clearly maintained. Neural signatures in the retention period could only be observed for attended WM contents, but not for unattended WM content (LaRocque et al., 2013; Lewis-Peacock et al., 2012). Thus, neuronal activity of the prefrontal area observed in the retention period might not reflect WM mechanisms, but rather the focus of attention.

Moreover, WM mechanisms might underlie certain neural states that cannot be traced with EEG methods (Sreenivasan et al., 2014; Stokes, 2015; Wolff et al., 2017). In other words, memory content might not be an explicit representation in a persistent activity state as hitherto assumed, but a more general neuronal response (Wolff et al., 2017). This may be the case of changes of functional connectivity within already established neuronal networks (Stokes, 2015). This framework highlights WM as a flexible and task-adaptable cognitive system, which can be dynamically reestablished (Wolff et al., 2017).

Instead of neuronal firing and measurable oscillations, those changes of functional connectivity for WM might also underlie short-term changes in synaptic

plasticity. Here, WM content is thought to be embedded in synaptic weights, an activity-silent model that is energetically far more efficient than persistent firing (Mongillo et al., 2008; Sreenivasan et al., 2014). Other ideas for hidden states include changes in extracellular transmitter concentrations or neuronal membrane potentials (Wolff et al., 2017).

Eventually, the exact mechanisms of WM and the functional relevance of neuronal oscillations for this cognitive system specifically are not fully understood and still need to be explored in future studies before intervening in WM processing and thus successfully enabling modulation of cognitive output.

5 Summary

In this study, we used brain state-dependent EEG-triggered transcranial magnetic stimulation (TMS) to target predefined phases of prefrontal theta oscillation with the attempt to modulate working memory performance of healthy human subjects in real time. For the real-time phase detection and estimation, we used an individualized spatial filter based on the MRI and EEG recording of each subject in order to source-project theta oscillations in the prefrontal cortical area.

Subjects were enrolled in two sessions of randomized order with different cortical stimulation targets (right posterior-parietal cortex/left dorsomedial prefrontal cortex). Throughout the session, EEG was recorded with a 126-channel EEG cap. Subjects were instructed to perform two different types of working memory tasks on a monitor with a handheld response box (Sternberg, visuospatial). TMS triple pulses (100Hz, 120% RMT, active condition) and electrical pulses (sham condition) were applied to the respective cortical targets during the retention period of the working memory tasks, either at the timepoint of prefrontal theta trough or of any random phase. Responses and response times of the working memory tasks were recorded.

In our study, the phase accuracy of TMS pulses was comparable to other brain state-dependent real-time EEG-TMS studies. TMS in the trough of the prefrontal theta oscillation did not affect working memory performance in comparison to the random phase. No significant difference regarding response accuracies and response times between TMS application in the trough and in the random phase of theta oscillations could be achieved in the real-time results. Significant differences were neither found by stimulating the right posterior-parietal cortex, nor the left dorsomedial prefrontal cortex. Post-hoc results did not yield significant phase correlations between response accuracy and different phases of prefrontal theta oscillation and posterior-parietal alpha oscillation.

These negative results inevitably lead to the revisit of current understandings of working memory function. Neuronal oscillations in the theta band might reflect

attentional processes in the WM processing system. Thus, working memory processing might only be sensitive to oscillatory effects in earlier stages, e.g. the encoding period, whereas in the retention period, dynamic changes in hidden brain states might portray a more efficient and robust method for maintaining working memory content.

6 German summary

In dieser Studie nutzten wir die durch EEG-Echtzeitanalyse ermöglichte hirnzustandsabhängige transkranielle Magnetstimulation (TMS), um vordefinierte Phasen der präfrontalen Theta-Oszillation gezielt anzusteuern mit dem Ziel, die Leistung des Arbeitsgedächtnisses von gesunden ProbandInnen zu modulieren. Für die Erkennung und Schätzung der Phasen in Echtzeit verwendeten wir einen individualisierten räumlichen Filter, der auf den MRT- und EEG-Aufzeichnungen der einzelnen ProbandInnen basierte, um auf die Quellaktivität der Theta-Oszillationen im präfrontalen Kortikalbereich zu schließen.

Die ProbandInnen nahmen an zwei Sitzungen in randomisierter Reihenfolge mit unterschiedlichen kortikalen Stimulationszielen teil (rechter posterior-parietaler Kortex/linker dorsomedialer präfrontaler Kortex). Während einer Sitzung erfolgte die kontinuierliche EEG-Aufzeichnung mit einer 126-Kanal EEG-Kappe. Die ProbandInnen wurden angewiesen, zwei Typen von Arbeitsgedächtnisaufgaben (Sternberg, räumlich) auf einem Monitor mit einer Hand-Antwortbox durchzuführen. TMS-Pulstriplets (100Hz, 120% RMT, aktive Bedingung) und elektrische Pulse (Scheinbedingung) wurden auf die entsprechenden kortikalen Ziele während der Retentionszeit der Arbeitsgedächtnisaufgaben entweder zum Zeitpunkt des präfrontalen Thetaminimums oder zufälliger Phase ausgelöst. Antworten und Antwortzeiten der Arbeitsgedächtnisaufgaben wurden aufgezeichnet.

In unserer Studie zeigte sich die Phasengenauigkeit der TMS-Pulse vergleichbar zu anderen hirnzustandsabhängigen EEG-TMS Studien. TMS im Minimum der präfrontalen Theta-Oszillation hatte keinen Einfluss auf die Leistung des

Arbeitsgedächtnisses im Vergleich zur zufälligen Phase. In den Echtzeit-Ergebnissen konnte kein signifikanter Unterschied hinsichtlich der Antwortgenauigkeit und der Antwortzeiten zwischen der TMS-Anwendung im Minimum und in der zufälligen Phase der Theta-Oszillationen festgestellt werden. Signifikante Unterschiede konnten weder für den rechten posterior-parietalen Kortex, noch für den linken dorsomedialen präfrontalen Kortex gefunden werden. Post-hoc-Ergebnisse deuten auf keine signifikanten Phasenkorrelationen zwischen Antwortgenauigkeit und verschiedenen Phasen der präfrontalen Theta-Oszillation und der posterior-parietalen Alpha-Oszillation hin.

Diese negativen Ergebnisse führen zu einem Überdenken des derzeitigen Verständnisses über die Funktionsweise des Arbeitsgedächtnisses. Neuronale Oszillationen im Theta-Band könnten Aufmerksamkeitsprozesse im WM-Verarbeitungssystem widerspiegeln. So könnte die Verarbeitung des Arbeitsgedächtnisses nur in früheren Phasen, z. B. in der Enkodierungsphase, für oszillatorische Effekte empfindlich sein, während in der Retentionsphase dynamische Veränderungen in dem EEG verborgenen Hirnzuständen eine effizientere und robustere Methode zur Aufrechterhaltung von Arbeitsgedächtnisinhalten darstellen könnten.

7 References

Abler, B., Walter, H., Wunderlich, A., Grothe, J., Schonfeldt-Lecuona, C., Spitzer, M., & Herwig, U. (2005). Side effects of transcranial magnetic stimulation biased task performance in a cognitive neuroscience study. *Brain Topogr*, *17*(4), 193-196. https://doi.org/10.1007/s10548-005-6028-y

Andersen, R. A. (1997). Multimodal integration for the representation of space in the posterior parietal cortex. *Philos Trans R Soc Lond B Biol Sci*, *352*(1360), 1421-1428. https://doi.org/10.1098/rstb.1997.0128

Axmacher, N., Henseler, M. M., Jensen, O., Weinreich, I., Elger, C. E., & Fell, J. (2010). Cross-frequency coupling supports multi-item working memory in the human hippocampus. *Proc Natl Acad Sci U S A*, *107*(7), 3228-3233. https://doi.org/10.1073/pnas.0911531107

Baddeley, A. (1992). Working memory. *Science*, *255*(5044), 556-559. https://doi.org/10.1126/science.1736359

Baetens, K., Ma, N., & Van Overwalle, F. (2017). The Dorsal Medial Prefrontal Cortex Is Recruited by High Construal of Non-social Stimuli. *Frontiers in Behavioral Neuroscience*, *11*. https://doi.org/10.3389/fnbeh.2017.00044

Belluscio, M. A., Mizuseki, K., Schmidt, R., Kempter, R., & Buzsaki, G. (2012). Cross-frequency phase-phase coupling between theta and gamma oscillations in the hippocampus. *J Neurosci*, *32*(2), 423-435. https://doi.org/10.1523/JNEUROSCI.4122-11.2012

Benchenane, K., Tiesinga, P. H., & Battaglia, F. P. (2011). Oscillations in the prefrontal cortex: a gateway to memory and attention. *Curr Opin Neurobiol*, *21*(3), 475-485. https://doi.org/10.1016/j.conb.2011.01.004

Berger, B., Griesmayr, B., Minarik, T., Biel, A. L., Pinal, D., Sterr, A., & Sauseng, P. (2019). Dynamic regulation of interregional cortical communication by slow brain oscillations during working memory. *Nat Commun*, *10*(1), 4242. https://doi.org/10.1038/s41467-019-12057-0

Bragin, A., Jando, G., Nadasdy, Z., Hetke, J., Wise, K., & Buzsaki, G. (1995). Gamma (40-100 Hz) oscillation in the hippocampus of the behaving rat. *J Neurosci*, *15*(1 Pt 1), 47-60. https://doi.org/10.1523/JNEUROSCI.15-01-00047.1995

Busch, N. A., & VanRullen, R. (2010). Spontaneous EEG oscillations reveal periodic sampling of visual attention. *Proc Natl Acad Sci U S A*, *107*(37), 16048-16053. https://doi.org/10.1073/pnas.1004801107

Buschman, T. J., & Miller, E. K. (2007). Top-down versus bottom-up control of attention in the prefrontal and posterior parietal cortices. *Science*, *315*(5820), 1860-1862. https://doi.org/10.1126/science.1138071

Buzsaki, G., Anastassiou, C. A., & Koch, C. (2012). The origin of extracellular fields and currents--EEG, ECoG, LFP and spikes. *Nat Rev Neurosci*, *13*(6), 407-420. https://doi.org/10.1038/nrn3241

Buzsaki, G., & Draguhn, A. (2004). Neuronal oscillations in cortical networks. *Science*, *304*(5679), 1926-1929. https://doi.org/10.1126/science.1099745

Buzsáki, G., & Moser, E. I. (2013). Memory, navigation and theta rhythm in the hippocampal-entorhinal system. *Nature Neuroscience*, *16*(2), 130-138. https://doi.org/10.1038/nn.3304

Buzsaki, G., & Wang, X. J. (2012). Mechanisms of gamma oscillations. *Annu Rev Neurosci*, *35*, 203-225. https://doi.org/10.1146/annurev-neuro-062111-150444

Cabeza, R., & Nyberg, L. (1997). Imaging Cognition: An Empirical Review of PET Studies with Normal Subjects. *J Cogn Neurosci*, *9*(1), 1-26. https://doi.org/10.1162/jocn.1997.9.1.1

Carvalhaes, C., & de Barros, J. A. (2015). The surface Laplacian technique in EEG: Theory and methods. *Int J Psychophysiol*, *97*(3), 174-188. https://doi.org/10.1016/j.ijpsycho.2015.04.023

Cavanagh, J. F., & Frank, M. J. (2014). Frontal theta as a mechanism for cognitive control. *Trends Cogn Sci*, *18*(8), 414-421. https://doi.org/10.1016/j.tics.2014.04.012

Clark, C. R., Moores, K. A., Lewis, A., Weber, D. L., Fitzgibbon, S., Greenblatt, R., Brown, G., & Taylor, J. (2001). Cortical network dynamics during verbal working memory function. *International Journal of Psychophysiology*, *42*(2), 161-176. https://doi.org/Doi 10.1016/S0167-8760(01)00164-7

Cohen, L. G., Roth, B. J., Nilsson, J., Dang, N., Panizza, M., Bandinelli, S., Friauf, W., & Hallett, M. (1990). Effects of Coil Design on Delivery of Focal Magnetic Stimulation - Technical Considerations. *Electroencephalography and Clinical Neurophysiology*, *75*(4), 350-357. https://doi.org/Doi 10.1016/0013-4694(90)90113-X

Colom, L. V., Christie, B. R., & Bland, B. H. (1988). Cingulate cell discharge patterns related to hippocampal EEG and their modulation by muscarinic and nicotinic agents. *Brain Res*, *460*(2), 329-338. https://doi.org/10.1016/0006-8993(88)90377-0

Corbetta, M. (1998). Frontoparietal cortical networks for directing attention and the eye to visual locations: identical, independent, or overlapping neural systems? *Proc Natl Acad Sci U S A*, *95*(3), 831-838. https://doi.org/10.1073/pnas.95.3.831

Corbetta, M., & Shulman, G. L. (2002). Control of goal-directed and stimulus-driven attention in the brain. *Nat Rev Neurosci*, *3*(3), 201-215. https://doi.org/10.1038/nrn755

Courtney, S. M., Petit, L., Maisog, J. M., Ungerleider, L. G., & Haxby, J. V. (1998). An area specialized for spatial working memory in human frontal cortex. *Science*, *279*(5355), 1347-1351. https://doi.org/10.1126/science.279.5355.1347

Courtney, S. M., Ungerleider, L. G., Keil, K., & Haxby, J. V. (1997). Transient and sustained activity in a distributed neural system for human working memory. *Nature*, *386*(6625), 608-611. https://doi.org/10.1038/386608a0

Cowan, N. (1995). Attention and memory: An integrated framework. *Oxford psychology series*, *26*.

Cowan, N. (2014). Working Memory Underpins Cognitive Development, Learning, and Education. *Educ Psychol Rev*, *26*(2), 197-223. https://doi.org/10.1007/s10648-013-9246-y

Culham, J. C., & Kanwisher, N. G. (2001). Neuroimaging of cognitive functions in human parietal cortex. *Curr Opin Neurobiol*, *11*(2), 157-163. https://doi.org/10.1016/s0959-4388(00)00191-4

Curtis, C. E., & D'Esposito, M. (2003). Persistent activity in the prefrontal cortex during working memory. *Trends Cogn Sci*, *7*(9), 415-423. https://doi.org/10.1016/s1364-6613(03)00197-9

D'Esposito, M., Aguirre, G. K., Zarahn, E., Ballard, D., Shin, R. K., & Lease, J. (1998). Functional MRI studies of spatial and nonspatial working memory. *Brain Res Cogn Brain Res*, *7*(1), 1-13. https://doi.org/10.1016/s0926-6410(98)00004-4

D'Esposito, M., & Postle, B. R. (2015). The cognitive neuroscience of working memory. *Annu Rev Psychol*, *66*, 115-142. https://doi.org/10.1146/annurev-psych-010814-015031

D'Esposito, M., Postle, B. R., & Rypma, B. (2000). Prefrontal cortical contributions to working memory: evidence from event-related

fMRI studies. *Exp Brain Res*, *133*(1), 3-11. https://doi.org/10.1007/s002210000395
Deserno, L., Sterzer, P., Wustenberg, T., Heinz, A., & Schlagenhauf, F. (2012). Reduced prefrontal-parietal effective connectivity and working memory deficits in schizophrenia. *J Neurosci*, *32*(1), 12-20. https://doi.org/10.1523/JNEUROSCI.3405-11.2012
Donoghue, T., Haller, M., Peterson, E. J., Varma, P., Sebastian, P., Gao, R., Noto, T., Lara, A. H., Wallis, J. D., Knight, R. T., Shestyuk, A., & Voytek, B. (2020). Parameterizing neural power spectra into periodic and aperiodic components. *Nat Neurosci*, *23*(12), 1655-1665. https://doi.org/10.1038/s41593-020-00744-x
Duprez, J., Gulbinaite, R., & Cohen, M. X. (2020). Midfrontal theta phase coordinates behaviorally relevant brain computations during cognitive control. *Neuroimage*, *207*, 116340. https://doi.org/10.1016/j.neuroimage.2019.116340
Feenstra, B. W., & Holsheimer, J. (1979). Dipole-like neuronal sources of theta rhythm in dorsal hippocampus, dentate gyrus and cingulate cortex of the urethane-anesthetized rat. *Electroencephalogr Clin Neurophysiol*, *47*(5), 532-538. https://doi.org/10.1016/0013-4694(79)90254-2
Fiebelkorn, I. C., & Kastner, S. (2019). A Rhythmic Theory of Attention. *Trends Cogn Sci*, *23*(2), 87-101. https://doi.org/10.1016/j.tics.2018.11.009
Fiebelkorn, I. C., Pinsk, M. A., & Kastner, S. (2018). A Dynamic Interplay within the Frontoparietal Network Underlies Rhythmic Spatial Attention. *Neuron*, *99*(4), 842-853 e848. https://doi.org/10.1016/j.neuron.2018.07.038
Fischl, B. (2012). FreeSurfer. *Neuroimage*, *62*(2), 774-781. https://doi.org/10.1016/j.neuroimage.2012.01.021
Friedman, H. R., & Goldman-Rakic, P. S. (1994). Coactivation of prefrontal cortex and inferior parietal cortex in working memory tasks revealed by 2DG functional mapping in the rhesus monkey. *J Neurosci*, *14*(5 Pt 1), 2775-2788. https://doi.org/10.1523/JNEUROSCI.14-05-02775.1994
Fries, P. (2015). Rhythms for Cognition: Communication through Coherence. *Neuron*, *88*(1), 220-235. https://doi.org/10.1016/j.neuron.2015.09.034
Fuster, J. M., & Alexander, G. E. (1971). Neuron activity related to short-term memory. *Science*, *173*(3997), 652-654. https://doi.org/10.1126/science.173.3997.652

Galhardoni, R., Correia, G. S., Araujo, H., Yeng, L. T., Fernandes, D. T., Kaziyama, H. H., Marcolin, M. A., Bouhassira, D., Teixeira, M. J., & de Andrade, D. C. (2015). Repetitive transcranial magnetic stimulation in chronic pain: a review of the literature. *Arch Phys Med Rehabil*, *96*(4 Suppl), S156-172. https://doi.org/10.1016/j.apmr.2014.11.010

Gevins, A., Smith, M. E., Leong, H., McEvoy, L., Whitfield, S., Du, R., & Rush, G. (1998). Monitoring working memory load during computer-based tasks with EEG pattern recognition methods. *Hum Factors*, *40*(1), 79-91. https://doi.org/10.1518/001872098779480578

Gevins, A., Smith, M. E., McEvoy, L. K., Leong, H., & Le, J. (1999). Electroencephalographic imaging of higher brain function. *Philos Trans R Soc Lond B Biol Sci*, *354*(1387), 1125-1133. https://doi.org/10.1098/rstb.1999.0468

Goldman-Rakic, P. S. (1987). Circuitry of the frontal association cortex and its relevance to dementia. *Archives of Gerontology and Geriatrics*, *6*(3), 299-309. https://doi.org/https://doi.org/10.1016/0167-4943(87)90029-X

Gopan, K. G., Prabhu, S. S., & Sinha, N. (2020). Sleep EEG analysis utilizing inter-channel covariance matrices. *Biocybernetics and Biomedical Engineering*, *40*(1), 527-545. https://doi.org/10.1016/j.bbe.2020.01.013

Gordon, P. C., Belardinelli, P., Stenroos, M., Ziemann, U., & Zrenner, C. (2022). Prefrontal theta phase-dependent rTMS-induced plasticity of cortical and behavioral responses in human cortex. *Brain Stimul*, *15*(2), 391-402. https://doi.org/10.1016/j.brs.2022.02.006

Gordon, P. C., Dorre, S., Belardinelli, P., Stenroos, M., Zrenner, B., Ziemann, U., & Zrenner, C. (2021). Prefrontal Theta-Phase Synchronized Brain Stimulation With Real-Time EEG-Triggered TMS. *Front Hum Neurosci*, *15*, 691821. https://doi.org/10.3389/fnhum.2021.691821

Grech, R., Cassar, T., Muscat, J., Camilleri, K. P., Fabri, S. G., Zervakis, M., Xanthopoulos, P., Sakkalis, V., & Vanrumste, B. (2008). Review on solving the inverse problem in EEG source analysis. *J Neuroeng Rehabil*, *5*, 25. https://doi.org/10.1186/1743-0003-5-25

Gregoriou, G. G., Gotts, S. J., Zhou, H., & Desimone, R. (2009). High-frequency, long-range coupling between prefrontal and visual

cortex during attention. *Science*, *324*(5931), 1207-1210. https://doi.org/10.1126/science.1171402
Hakim, N., Feldmann-Wustefeld, T., Awh, E., & Vogel, E. K. (2021). Controlling the Flow of Distracting Information in Working Memory. *Cereb Cortex*, *31*(7), 3323-3337. https://doi.org/10.1093/cercor/bhab013
Hallett, M. (2007). Transcranial magnetic stimulation: a primer. *Neuron*, *55*(2), 187-199. https://doi.org/10.1016/j.neuron.2007.06.026
Hallez, H., Vanrumste, B., Grech, R., Muscat, J., De Clercq, W., Vergult, A., D'Asseler, Y., Camilleri, K. P., Fabri, S. G., Van Huffel, S., & Lemahieu, I. (2007). Review on solving the forward problem in EEG source analysis. *J Neuroeng Rehabil*, *4*, 46. https://doi.org/10.1186/1743-0003-4-46
Hutcheon, B., & Yarom, Y. (2000). Resonance, oscillation and the intrinsic frequency preferences of neurons. *Trends Neurosci*, *23*(5), 216-222. https://doi.org/10.1016/s0166-2236(00)01547-2
Ishii, R., Shinosaki, K., Ukai, S., Inouye, T., Ishihara, T., Yoshimine, T., Hirabuki, N., Asada, H., Kihara, T., Robinson, S. E., & Takeda, M. (1999). Medial prefrontal cortex generates frontal midline theta rhythm. *Neuroreport*, *10*(4), 675-679. https://doi.org/10.1097/00001756-199903170-00003
Jackson, A. F., & Bolger, D. J. (2014). The neurophysiological bases of EEG and EEG measurement: a review for the rest of us. *Psychophysiology*, *51*(11), 1061-1071. https://doi.org/10.1111/psyp.12283
Jackson, S. R., & Husain, M. (2006). Visuomotor functions of the posterior parietal cortex. *Neuropsychologia*, *44*(13), 2589-2593. https://doi.org/10.1016/j.neuropsychologia.2006.08.002
Jensen, O., & Lisman, J. E. (2000). Position reconstruction from an ensemble of hippocampal place cells: contribution of theta phase coding. *J Neurophysiol*, *83*(5), 2602-2609. https://doi.org/10.1152/jn.2000.83.5.2602
Jensen, O., & Tesche, C. D. (2002). Frontal theta activity in humans increases with memory load in a working memory task. *Eur J Neurosci*, *15*(8), 1395-1399. https://doi.org/10.1046/j.1460-9568.2002.01975.x
Jimura, K., Chushak, M. S., Westbrook, A., & Braver, T. S. (2018). Intertemporal Decision-Making Involves Prefrontal Control

Mechanisms Associated with Working Memory. *Cereb Cortex*, *28*(4), 1105-1116. https://doi.org/10.1093/cercor/bhx015

Jonides, J., Smith, E. E., Koeppe, R. A., Awh, E., Minoshima, S., & Mintun, M. A. (1993). Spatial Working-Memory in Humans as Revealed by Pet. *Nature*, *363*(6430), 623-625. https://doi.org/DOI 10.1038/363623a0

Kahana, M. J., Sekuler, R., Caplan, J. B., Kirschen, M., & Madsen, J. R. (1999). Human theta oscillations exhibit task dependence during virtual maze navigation. *Nature*, *399*(6738), 781-784. https://doi.org/10.1038/21645

Kim, C., Kroger, J. K., Calhoun, V. D., & Clark, V. P. (2015). The role of the frontopolar cortex in manipulation of integrated information in working memory. *Neurosci Lett*, *595*, 25-29. https://doi.org/10.1016/j.neulet.2015.03.044

Klausberger, T., Marton, L. F., Baude, A., Roberts, J. D., Magill, P. J., & Somogyi, P. (2004). Spike timing of dendrite-targeting bistratified cells during hippocampal network oscillations in vivo. *Nat Neurosci*, *7*(1), 41-47. https://doi.org/10.1038/nn1159

Klimesch, W., Fellinger, R., & Freunberger, R. (2011). Alpha oscillations and early stages of visual encoding. *Front Psychol*, *2*, 118. https://doi.org/10.3389/fpsyg.2011.00118

Klimesch, W., Schimke, H., & Schwaiger, J. (1994). Episodic and semantic memory: an analysis in the EEG theta and alpha band. *Electroencephalogr Clin Neurophysiol*, *91*(6), 428-441. https://doi.org/10.1016/0013-4694(94)90164-3

Kobayashi, M., & Pascual-Leone, A. (2003). Transcranial magnetic stimulation in neurology. *Lancet Neurol*, *2*(3), 145-156. https://doi.org/10.1016/s1474-4422(03)00321-1

LaRocque, J. J., Lewis-Peacock, J. A., Drysdale, A. T., Oberauer, K., & Postle, B. R. (2013). Decoding attended information in short-term memory: an EEG study. *J Cogn Neurosci*, *25*(1), 127-142. https://doi.org/10.1162/jocn_a_00305

Lasztoczi, B., & Klausberger, T. (2014). Layer-specific GABAergic control of distinct gamma oscillations in the CA1 hippocampus. *Neuron*, *81*(5), 1126-1139. https://doi.org/10.1016/j.neuron.2014.01.021

Lewis-Peacock, J. A., Drysdale, A. T., Oberauer, K., & Postle, B. R. (2012). Neural evidence for a distinction between short-term memory and the focus of attention. *J Cogn Neurosci*, *24*(1), 61-79. https://doi.org/10.1162/jocn_a_00140

Lisman, J. E., & Jensen, O. (2013). The theta-gamma neural code. *Neuron*, *77*(6), 1002-1016. https://doi.org/10.1016/j.neuron.2013.03.007

Liu, D., Wang, Q., Zhang, Y., Liu, X., Lu, J., & Sun, J. (2019). A study on quality assessment of the surface EEG signal based on fuzzy comprehensive evaluation method. *Comput Assist Surg (Abingdon)*, *24*(sup1), 167-173. https://doi.org/10.1080/24699322.2018.1557888

Llinas, R. R. (1988). The intrinsic electrophysiological properties of mammalian neurons: insights into central nervous system function. *Science*, *242*(4886), 1654-1664. https://doi.org/10.1126/science.3059497

Lopez-Alonso, V., Cheeran, B., Rio-Rodriguez, D., & Fernandez-Del-Olmo, M. (2014). Inter-individual variability in response to non-invasive brain stimulation paradigms. *Brain Stimul*, *7*(3), 372-380. https://doi.org/10.1016/j.brs.2014.02.004

Lorenc, E. S., Mallett, R., & Lewis-Peacock, J. A. (2021). Distraction in Visual Working Memory: Resistance is Not Futile. *Trends Cogn Sci*, *25*(3), 228-239. https://doi.org/10.1016/j.tics.2020.12.004

Lutzenberger, W., Ripper, B., Busse, L., Birbaumer, N., & Kaiser, J. (2002). Dynamics of gamma-band activity during an audiospatial working memory task in humans. *J Neurosci*, *22*(13), 5630-5638. https://doi.org/10.1523/JNEUROSCI.22-13-05630.2002

Malhotra, P., Coulthard, E. J., & Husain, M. (2009). Role of right posterior parietal cortex in maintaining attention to spatial locations over time. *Brain*, *132*(Pt 3), 645-660. https://doi.org/10.1093/brain/awn350

Manoach, D. S., Schlaug, G., Siewert, B., Darby, D. G., Bly, B. M., Benfield, A., Edelman, R. R., & Warach, S. (1997). Prefrontal cortex fMRI signal changes are correlated with working memory load. *Neuroreport*, *8*(2), 545-549. https://doi.org/10.1097/00001756-199701200-00033

Melrose, R. J., Zahniser, E., Wilkins, S. S., Veliz, J., Hasratian, A. S., Sultzer, D. L., & Jimenez, A. M. (2020). Prefrontal working memory activity predicts episodic memory performance: A neuroimaging study. *Behav Brain Res*, *379*, 112307. https://doi.org/10.1016/j.bbr.2019.112307

Meshulam, M., Ramot, M., Harel, M., Kipervasser, S., Andelman, F., Neufeld, M. Y., Kramer, U., Fried, I., & Malach, R. (2013).

Selectivity of audiovisual ECoG responses revealed under naturalistic stimuli in the human cortex. *J Neurophysiol*, *109*(9), 2272-2281. https://doi.org/10.1152/jn.00474.2012

Miller, E. K., & Cohen, J. D. (2001). An integrative theory of prefrontal cortex function. *Annu Rev Neurosci*, *24*, 167-202. https://doi.org/10.1146/annurev.neuro.24.1.167

Mitchell, D. J., McNaughton, N., Flanagan, D., & Kirk, I. J. (2008). Frontal-midline theta from the perspective of hippocampal "theta". *Prog Neurobiol*, *86*(3), 156-185. https://doi.org/10.1016/j.pneurobio.2008.09.005

Mongillo, G., Barak, O., & Tsodyks, M. (2008). Synaptic theory of working memory. *Science*, *319*(5869), 1543-1546. https://doi.org/10.1126/science.1150769

Morgan, H. M., Muthukumaraswamy, S. D., Hibbs, C. S., Shapiro, K. L., Bracewell, R. M., Singh, K. D., & Linden, D. E. (2011). Feature integration in visual working memory: parietal gamma activity is related to cognitive coordination. *J Neurophysiol*, *106*(6), 3185-3194. https://doi.org/10.1152/jn.00246.2011

Mueller-Buehl, C., Wegrzyn, D., Bauch, J., & Faissner, A. (2023). Regulation of the E/I-balance by the neural matrisome. *Frontiers in Molecular Neuroscience*, *16*. https://doi.org/ARTN 1102334

10.3389/fnmol.2023.1102334

Muller-Dahlhaus, J. F., Orekhov, Y., Liu, Y., & Ziemann, U. (2008). Interindividual variability and age-dependency of motor cortical plasticity induced by paired associative stimulation. *Exp Brain Res*, *187*(3), 467-475. https://doi.org/10.1007/s00221-008-1319-7

Narayana, S., Gibbs, S. K., Fulton, S. P., McGregor, A. L., Mudigoudar, B., Weatherspoon, S. E., Boop, F. A., & Wheless, J. W. (2021). Clinical Utility of Transcranial Magnetic Stimulation (TMS) in the Presurgical Evaluation of Motor, Speech, and Language Functions in Young Children With Refractory Epilepsy or Brain Tumor: Preliminary Evidence. *Front Neurol*, *12*, 650830. https://doi.org/10.3389/fneur.2021.650830

Nummenmaa, A., Stenroos, M., Ilmoniemi, R. J., Okada, Y. C., Hamalainen, M. S., & Raij, T. (2013). Comparison of spherical and realistically shaped boundary element head models for transcranial magnetic stimulation navigation. *Clin Neurophysiol*,

124(10), 1995-2007. https://doi.org/10.1016/j.clinph.2013.04.019

Nunez, P. L. (1996). The electroencephalograph. Its patterns and origins - Barlow,JS. *Psychophysiology*, *33*(4), 476-477. <Go to ISI>://WOS:A1996UU13300017

Ojemann, G. A., Ojemann, J., & Ramsey, N. F. (2013). Relation between functional magnetic resonance imaging (fMRI) and single neuron, local field potential (LFP) and electrocorticography (ECoG) activity in human cortex. *Frontiers in Human Neuroscience*, *7*. https://doi.org/ARTN 34
10.3389/fnhum.2013.00034

Olesen, P. J., Westerberg, H., & Klingberg, T. (2004). Increased prefrontal and parietal activity after training of working memory. *Nat Neurosci*, *7*(1), 75-79. https://doi.org/10.1038/nn1165

Oostenveld, R., Fries, P., Maris, E., & Schoffelen, J. M. (2011). FieldTrip: Open source software for advanced analysis of MEG, EEG, and invasive electrophysiological data. *Comput Intell Neurosci*, *2011*, 156869. https://doi.org/10.1155/2011/156869

Osaka, N., Osaka, M., Kondo, H., Morishita, M., Fukuyama, H., & Shibasaki, H. (2004). The neural basis of executive function in working memory: an fMRI study based on individual differences. *Neuroimage*, *21*(2), 623-631. https://doi.org/10.1016/j.neuroimage.2003.09.069

Penttonen, M., Kamondi, A., Acsady, L., & Buzsaki, G. (1998). Gamma frequency oscillation in the hippocampus of the rat: intracellular analysis in vivo. *Eur J Neurosci*, *10*(2), 718-728. https://doi.org/10.1046/j.1460-9568.1998.00096.x

Piva, M., Velnoskey, K., Jia, R., Nair, A., Levy, I., & Chang, S. W. (2019). The dorsomedial prefrontal cortex computes task-invariant relative subjective value for self and other. *Elife*, *8*. https://doi.org/10.7554/eLife.44939

Raghavachari, S., Kahana, M. J., Rizzuto, D. S., Caplan, J. B., Kirschen, M. P., Bourgeois, B., Madsen, J. R., & Lisman, J. E. (2001). Gating of human theta oscillations by a working memory task. *J Neurosci*, *21*(9), 3175-3183. https://doi.org/10.1523/JNEUROSCI.21-09-03175.2001

Ragland, J. D., Turetsky, B. I., Gur, R. C., Gunning-Dixon, F., Turner, T., Schroeder, L., Chan, R., & Gur, R. E. (2002). Working memory for complex figures: an fMRI comparison of letter and fractal n-back tasks. *Neuropsychology*, *16*(3), 370-379. https://www.ncbi.nlm.nih.gov/pubmed/12146684

Rizzuto, D. S., Madsen, J. R., Bromfield, E. B., Schulze-Bonhage, A., Seelig, D., Aschenbrenner-Scheibe, R., & Kahana, M. J. (2003). Reset of human neocortical oscillations during a working memory task. *Proc Natl Acad Sci U S A*, *100*(13), 7931-7936. https://doi.org/10.1073/pnas.0732061100

Roux, F., & Uhlhaas, P. J. (2014). Working memory and neural oscillations: alpha-gamma versus theta-gamma codes for distinct WM information? *Trends Cogn Sci*, *18*(1), 16-25. https://doi.org/10.1016/j.tics.2013.10.010

Roznowski, M., & Smith, M. L. (1993). A Note on Some Psychometric Properties of Sternberg Task-Performance - Modifications to Content. *Intelligence*, *17*(3), 389-398. https://doi.org/Doi 10.1016/0160-2896(93)90006-Q

Ruddy, K. L., Woolley, D. G., Mantini, D., Balsters, J. H., Enz, N., & Wenderoth, N. (2018). Improving the quality of combined EEG-TMS neural recordings: Introducing the coil spacer. *J Neurosci Methods*, *294*, 34-39. https://doi.org/10.1016/j.jneumeth.2017.11.001

Russo, S., Sarasso, S., Puglisi, G., Pigorini, A., Casarotto, S., D'Ambrosio, S., Astolfi, A., Massimini, M., Rosanova, M., & Fecchio, M. (2021). *TAAC - TMS Adaptable Auditory Control: a universal tool to mask TMS click*. https://doi.org/10.1101/2021.09.08.459439

Sarnthein, J., Petsche, H., Rappelsberger, P., Shaw, G. L., & von Stein, A. (1998). Synchronization between prefrontal and posterior association cortex during human working memory. *Proc Natl Acad Sci U S A*, *95*(12), 7092-7096. https://doi.org/10.1073/pnas.95.12.7092

Sauseng, P., Griesmayr, B., Freunberger, R., & Klimesch, W. (2010). Control mechanisms in working memory: a possible function of EEG theta oscillations. *Neurosci Biobehav Rev*, *34*(7), 1015-1022. https://doi.org/10.1016/j.neubiorev.2009.12.006

Sauseng, P., Hoppe, J., Klimesch, W., Gerloff, C., & Hummel, F. C. (2007). Dissociation of sustained attention from central executive functions: local activity and interregional connectivity in the theta range. *Eur J Neurosci*, *25*(2), 587-593. https://doi.org/10.1111/j.1460-9568.2006.05286.x

Sauseng, P., Klimesch, W., Schabus, M., & Doppelmayr, M. (2005). Fronto-parietal EEG coherence in theta and upper alpha reflect central executive functions of working memory. *Int J*

Psychophysiol, *57*(2), 97-103. https://doi.org/10.1016/j.ijpsycho.2005.03.018

Siapas, A. G., Lubenov, E. V., & Wilson, M. A. (2005). Prefrontal phase locking to hippocampal theta oscillations. *Neuron*, *46*(1), 141-151. https://doi.org/10.1016/j.neuron.2005.02.028

Siegel, M., Warden, M. R., & Miller, E. K. (2009). Phase-dependent neuronal coding of objects in short-term memory. *Proc Natl Acad Sci U S A*, *106*(50), 21341-21346. https://doi.org/10.1073/pnas.0908193106

Smith, E. E., Jonides, J., & Koeppe, R. A. (1996). Dissociating verbal and spatial working memory using PET. *Cereb Cortex*, *6*(1), 11-20. https://doi.org/10.1093/cercor/6.1.11

Sreenivasan, K. K., Curtis, C. E., & D'Esposito, M. (2014). Revisiting the role of persistent neural activity during working memory. *Trends Cogn Sci*, *18*(2), 82-89. https://doi.org/10.1016/j.tics.2013.12.001

Stefanou, M. I., Desideri, D., Belardinelli, P., Zrenner, C., & Ziemann, U. (2018). Phase Synchronicity of mu-Rhythm Determines Efficacy of Interhemispheric Communication Between Human Motor Cortices. *J Neurosci*, *38*(49), 10525-10534. https://doi.org/10.1523/JNEUROSCI.1470-18.2018

Stenroos, M., & Sarvas, J. (2012). Bioelectromagnetic forward problem: isolated source approach revis(it)ed. *Phys Med Biol*, *57*(11), 3517-3535. https://doi.org/10.1088/0031-9155/57/11/3517

Sternberg, S. (1966). High-speed scanning in human memory. *Science*, *153*(3736), 652-654. https://doi.org/10.1126/science.153.3736.652

Sternberg, S. (1969). Memory-scanning: mental processes revealed by reaction-time experiments. *Am Sci*, *57*(4), 421-457. https://www.ncbi.nlm.nih.gov/pubmed/5360276

Stokes, M. G. (2015). 'Activity-silent' working memory in prefrontal cortex: a dynamic coding framework. *Trends Cogn Sci*, *19*(7), 394-405. https://doi.org/10.1016/j.tics.2015.05.004

Tarapore, P. E., Findlay, A. M., Honma, S. M., Mizuiri, D., Houde, J. F., Berger, M. S., & Nagarajan, S. S. (2013). Language mapping with navigated repetitive TMS: proof of technique and validation. *Neuroimage*, *82*, 260-272. https://doi.org/10.1016/j.neuroimage.2013.05.018

Van Veen, B. D., van Drongelen, W., Yuchtman, M., & Suzuki, A. (1997). Localization of brain electrical activity via linearly

constrained minimum variance spatial filtering. *IEEE Trans Biomed Eng*, *44*(9), 867-880. https://doi.org/10.1109/10.623056
VanRullen, R. (2016). Perceptual Cycles. *Trends Cogn Sci*, *20*(10), 723-735. https://doi.org/10.1016/j.tics.2016.07.006
von Stein, A., & Sarnthein, J. (2000). Different frequencies for different scales of cortical integration: from local gamma to long range alpha/theta synchronization. *International Journal of Psychophysiology*, *38*(3), 301-313. https://doi.org/Doi 10.1016/S0167-8760(00)00172-0
Wager, T. D., & Smith, E. E. (2003). Neuroimaging studies of working memory: a meta-analysis. *Cogn Affect Behav Neurosci*, *3*(4), 255-274. https://doi.org/10.3758/cabn.3.4.255
Wen, H., & Liu, Z. (2016). Broadband Electrophysiological Dynamics Contribute to Global Resting-State fMRI Signal. *J Neurosci*, *36*(22), 6030-6040. https://doi.org/10.1523/JNEUROSCI.0187-16.2016
Whitlock, J. R. (2017). Posterior parietal cortex. *Curr Biol*, *27*(14), R691-R695. https://doi.org/10.1016/j.cub.2017.06.007
Wolff, M. J., Jochim, J., Akyurek, E. G., & Stokes, M. G. (2017). Dynamic hidden states underlying working-memory-guided behavior. *Nat Neurosci*, *20*(6), 864-871. https://doi.org/10.1038/nn.4546
Young, C. K., & McNaughton, N. (2009). Coupling of theta oscillations between anterior and posterior midline cortex and with the hippocampus in freely behaving rats. *Cereb Cortex*, *19*(1), 24-40. https://doi.org/10.1093/cercor/bhn055
Zrenner, C., Desideri, D., Belardinelli, P., & Ziemann, U. (2018). Real-time EEG-defined excitability states determine efficacy of TMS-induced plasticity in human motor cortex. *Brain Stimul*, *11*(2), 374-389. https://doi.org/10.1016/j.brs.2017.11.016
Zrenner, C., Galevska, D., Nieminen, J. O., Baur, D., Stefanou, M. I., & Ziemann, U. (2020). The shaky ground truth of real-time phase estimation. *Neuroimage*, *214*, 116761. https://doi.org/10.1016/j.neuroimage.2020.116761

8 Declaration of Contributions

The work was carried out in the University Clinic for Neurology Tübingen under the supervision of Prof. Dr. Ulf Ziemann. The conception of this study was done in cooperation with Prof. Dr. Ulf Ziemann and Dr. Pedro C. Gordon. The experiments were carried out by me and Dr. Pedro C. Gordon.

The head models were created by Prof. Dr. Paolo Belardinelli, the experiment scripts were written by Dr. Christoph Zrenner, Dr. Pedro C. Gordon and Umair Hassan.

The data analysis was carried out by me and Dr. Pedro C. Gordon.

I hereby assure that the manuscript was entirely written by me and that I used no other references than those cited in the manuscript.

Tübingen, 01.10.2024

Elina Fanglin Song

9 Acknowledgements

I would like to thank Prof. Dr. Ulf Ziemann for providing me the opportunity to work on this research project in his lab and Dr. Pedro C. Gordon for his guidance and advice.

I would also like to thank the most amazing colleagues and friends Yufei, Maria and Johanna for their support and encouragement and my partner David.

My gratitude goes to all the subjects, who invested much of their time and patience to participate in this study.

I would not have made it that far without any of these wonderful people.

Thank you!